



**HAL**  
open science

# Stimuli-Responsive Metal Complexes for Biomedical Applications

Ivanna Amarsy, Sébastien Papot, Gilles Gasser

► **To cite this version:**

Ivanna Amarsy, Sébastien Papot, Gilles Gasser. Stimuli-Responsive Metal Complexes for Biomedical Applications. *Angewandte Chemie International Edition*, 2022, 61 (40), pp.e202205900. 10.1002/anie.202205900 . hal-03713992

**HAL Id: hal-03713992**

**<https://hal.science/hal-03713992>**

Submitted on 5 Jul 2022

**HAL** is a multi-disciplinary open access archive for the deposit and dissemination of scientific research documents, whether they are published or not. The documents may come from teaching and research institutions in France or abroad, or from public or private research centers.

L'archive ouverte pluridisciplinaire **HAL**, est destinée au dépôt et à la diffusion de documents scientifiques de niveau recherche, publiés ou non, émanant des établissements d'enseignement et de recherche français ou étrangers, des laboratoires publics ou privés.

# Stimuli-Responsive Metal Complexes for Biomedical Applications

Ivanna Amarsy,<sup>a</sup> Sébastien Papot<sup>b,\*</sup> and Gilles Gasser<sup>a,\*</sup>

<sup>a</sup> Chimie ParisTech, PSL University, CNRS, Institute of Chemistry for Life and Health Sciences, Laboratory for Inorganic Chemical Biology, F-75005 Paris, France. Email: [ivanna.amarsy@chimieparistech.psl.eu](mailto:ivanna.amarsy@chimieparistech.psl.eu) [gilles.gasser@chimieparistech.psl.eu](mailto:gilles.gasser@chimieparistech.psl.eu); [WWW: www.gassergroup.com](http://www.gassergroup.com)

<sup>b</sup> Institut de Chimie des Milieux et des Matériaux de Poitiers (IC2MP), Université de Poitiers, CNRS, 4 rue Michel Brunet, TSA 51106, F-86073 Poitiers, France. Equipe Labellisée Ligue Contre le Cancer. Email: [sebastien.papot@univ-poitiers.fr](mailto:sebastien.papot@univ-poitiers.fr).

## ORCID-ID:

Ivanna Amarsy: 0000-0002-7560-7830

Sébastien Papot: 0000-0001-5253-1979

Gilles Gasser: 0000-0002-4244-5097

**KEYWORDS:** Diagnostic tools, Drug Release; Medicinal Inorganic Chemistry; Metals in Medicine; Selective Delivery.

## Abbreviations

4ABA: 4-aminobenzyl alcohol, ADEPT: antibody direct enzyme prodrug therapy,  $\beta$ -gal:  $\beta$ -galactosidase,  $\beta$ -lac:  $\beta$ -lactamase,  $\beta$ -gluc:  $\beta$ -glucuronidase, BR: Biotin receptor, CA: contrast agent, CPT: camptothecin, cDDP: Cis-dichlorodiammineplatinum, DEPT: direct enzyme prodrug therapy, DO3A: 1,4,7-tris(carboxymethyl)-1,4,7,10-tetraazacyclododecane, FDA: Food and drug administration, GSH: glutathion, 7-HMC: 7-hydroxy-3-methylcoumarin, MeHC: methyl trans-2-hydroxycinnamate, MRI: magnetic resonance imaging, NO: nitric oxide, PARACEST: paramagnetic chemical exchange saturation transfer, PET: positron

emission tomography, QM: quinone methide, ROS: Reactive oxygen species, SPECT: Single photon emission computed tomography.

### **Abstract**

Metal-based compounds have been widely used for biomedical applications. Their unique characteristics make them attractive for both therapeutic and diagnostic purposes. However, numerous issues including toxicity, poor aqueous solubility, and unfavorable biodistribution hamper their widespread use. To overcome these drawbacks, the concept of metal-based prodrugs emerged. This field is particularly developed for applications in oncology. More precisely, tumor-associated stimuli (e.g., pH variation, redox activity, enzyme overexpression, etc.) have been exploited to trigger the selective delivery of active metal-based drugs to the tumor site. The main advances in this area are discussed in this review.

## Biographies



**Ivanna Amarsy** received her B.Sc. in Biology and Chemistry from Paris-Saclay University (Paris, France) in 2018 and her M.Sc. in organic chemistry from the same institute in 2020. She is currently a Ph.D. student in the research group of Prof. Gilles Gasser at Chimie Paris-Tech, PSL University (Paris, France) in co-supervision with Prof. Sébastien Papot from the University of Poitiers (France) studying the design and synthesis of metal-based anticancer complexes delivery system.



**Sébastien Papot** is Professor of organic chemistry at the University of Poitiers (France) where he is heading the Programmed Molecular Systems Team within the IC2MP (Institut de Chimie des Milieux et des Matériaux de Poitiers). Sébastien was the recipient of the Pierre Fabre Award for Therapeutic Innovation (2014). He was the President of the French Medicinal Chemistry Society (SCT, 2019-2020). Sébastien is also the co-founder and CSO of Seekyo, a biotechnology company developing new generation cancer treatments. His research interests include the design of smart drug delivery systems, *in vivo* chemistry, functional interlocked systems and prebiotic chemistry.



**Gilles Gasser** started his independent scientific career at the University of Zurich (Switzerland) in 2010 before moving to Chimie ParisTech, PSL University (Paris, France) in 2016 to take a PSL Chair of Excellence. Gilles was the recipient of several fellowships and awards including the Alfred Werner Award from the Swiss Chemical Society, an ERC Consolidator Grant, the European BioInorganic Chemistry (EuroBIC) medal and the Pierre Fabre Award for therapeutic innovation from the French Société de Chimie Thérapeutique. He is a Fellow of the Royal Society of Chemistry since 2021. Gilles' research interests lay in the use of metal complexes in different areas of medicinal and biological chemistry.

## 1. Introduction

Metals are present in all living organisms and play a fundamental role in a wide range of biological processes such as cofactors, enzymes (e.g., superoxide dismutase) or metal salts (iron, zinc, calcium, etc.).<sup>[1,2]</sup> This is likely one of the reasons why the use of metals for biomedical applications has attracted great interest for many centuries. For instance, the use of gold for therapeutic purposes has been reported in both the Egyptian and Chinese cultures about 4500 years ago.<sup>[3]</sup> However, it was only after the discovery of salvarsan, an arsenic-based antimicrobial agent effective against syphilis, by Paul Ehrlich in 1912 that the study of metals as potential drugs took off.<sup>[4]</sup>

One of the major breakthroughs that marked the interest in metallodrugs was the discovery of cisplatin in 1965 through serendipity by Barnett Rosenberg and Loretta VanCamp.<sup>[5]</sup> Cisplatin and its derivatives are currently among the most widely used drugs for cancer therapy.<sup>[4,6,7]</sup> Nowadays, a large number of metal complexes are employed for various medical applications (Figure 1). The two pnictogens, antimony and bismuth, are frequently prescribed as antimicrobial and antiparasitic agents, and also in the treatment of gastrointestinal disorders (i.e., the bismuth subsalicylate) (Figure 2).<sup>[4]</sup> Silver is commonly incorporated in creams and aqueous solutions to fight infections resulting from burns.<sup>[4]</sup> Gold is employed as an antiarthritic (auranofin)<sup>[8,9]</sup> (Figure 2) and even explored as a potential agent against infectious diseases and cancer.<sup>[1]</sup> Aside from their use in drugs, metal complexes are also utilized as diagnostic tools.

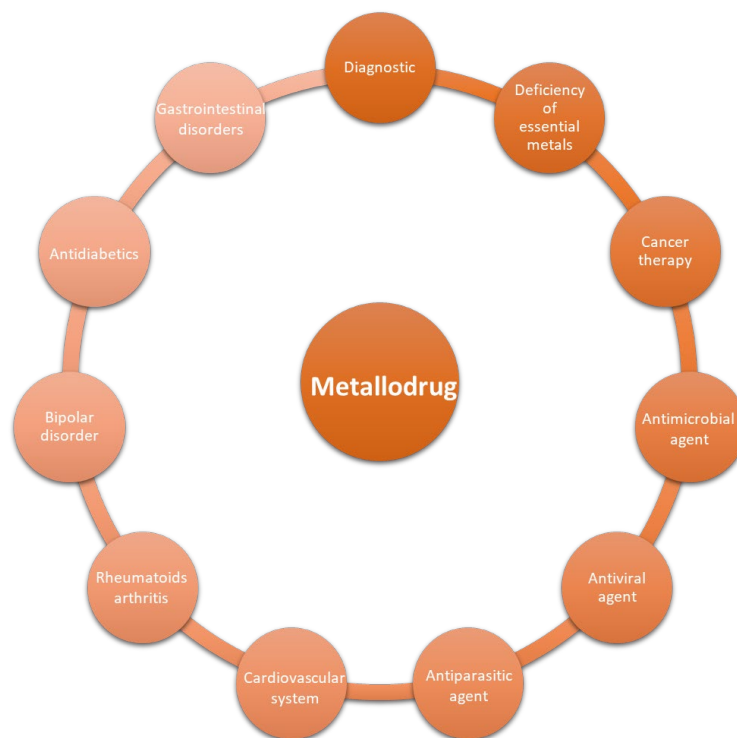


Figure 1. Representative diagram of the different applications of a metallo drug.

The dominant isotope, also called the “Workhorse of Diagnostic Nuclear Medicine” in SPECT and PET imaging, is *technetium-99m*, with twenty-eight  $^{99m}\text{Tc}$  imaging agents approved by the FDA so far. As for MRI scans, the most used metal is gadolinium, with few examples also approved by the FDA.<sup>[4]</sup> To demonstrate the importance of this metal ion, it is worth mentioning that 500,000 doses are given every day around the globe. One important issue that must be overcome in order to use this metal is the high toxicity of the free Gd(III) ion. In this context, the design of biocompatible complexes should prevent the release of the free metal ion *in vivo*, hence reducing its toxicity.<sup>[10–12]</sup>

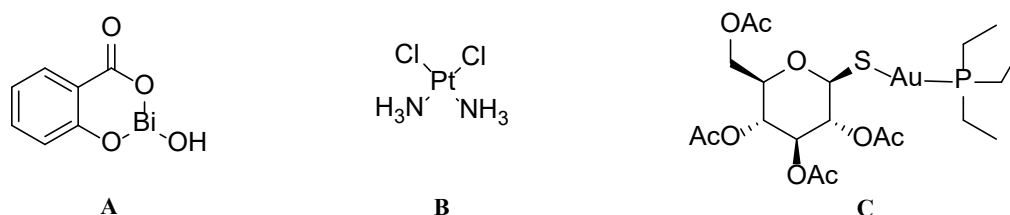


Figure 2. Examples of metallo drugs (A) bismuth subsalicylate (B) cisplatin (C) auranofin.



Compared to purely organic compounds, metal-containing derivatives present unique characteristics that confers several advantages for the design of bioactive molecules. First, metal centers exhibit various geometry (e.g., pyramidal, trigonal bipyramidal, octahedral, etc.) providing a greater stereochemical diversity than a tetrahedral carbon atom.<sup>[8,13,14]</sup> This diversity increases *de facto* the number of biological targets,<sup>[15]</sup> increases the possible interaction modes, and allows a better selectivity (e.g., targeting one specific kinase on the 518 coded by the human genome).<sup>[15,16]</sup> Second, the redox potential of metals allows them to manipulate biological processes (e.g., production of ROS).<sup>[3,4,14]</sup> It can also confer spectroscopic (e.g., Mossbauer spectroscopy), magnetic, or radioactive properties that find applications in therapy or diagnosis.<sup>[4]</sup> However, as it is the case with their organic counterparts, the use of metal complexes in the clinic is still fraught with numerous issues including toxicity, poor aqueous solubility, and unfavorable biodistribution.<sup>[1,8]</sup> For example, the widely used cisplatin lacks of selectivity leading to a severe kidney toxicity that limit its therapeutic efficacy.<sup>[1,5,17,18]</sup> With the aim to overcome these limitations, the concept of metal-based prodrugs was proposed in the 2000s.<sup>[19,20]</sup> As introduced earlier by Albert,<sup>[21]</sup> a prodrug is usually defined as a medication or compound that is metabolized into a pharmacologically active drug once administered in a living organism. This approach was specifically explored in cancer chemotherapy with the design of prodrugs that can be activated exclusively in malignant tissues. Within this framework, most of the anticancer prodrugs developed so far include a specific trigger that induces the release of the active drug in response to a tumor-associated stimulus (e.g., pH, redox, enzyme, etc.).<sup>[20,22,23]</sup> (Figure 3) The best illustrations of this strategy are the antibody-drug conjugates (ADCs) bearing a stimuli-responsive linker, with several of them already approved for various applications in oncology.<sup>[24-26]</sup>

The prodrug concept has been considered in the case of metallodrugs and some of them have already shown promising results with an increased selectivity and reduced side effects in clinical trials.<sup>[27],[28]</sup> For example, it was postulated that the Ruthenium complex NAMI-A, which has reached phase II clinical trial, was activated upon reduction in cells, – we note that this suggestion is under debate.<sup>[29,30]</sup> Several Pt(IV) complexes, like Straplatin, which are activated upon reduction, entered clinical trial. In addition, the approved Pt(II) complexes (e.g, cisplatin, carboplatin, oxaliplatin, etc.) and the liposome nanoparticle formulation of cisplatin, Lipoplatin, which successfully finished Phase III as treatment for non-small cell lung cancer adenocarcinomas, are other examples of prodrugs per se – they undergo aquation before binding to DNA.<sup>[31]</sup> In this review, we present the different stimuli-responsive metal complex delivery systems investigated to date for both therapeutic and diagnostic purposes. While photosensitizers (PSs) are sometimes considered as prodrugs, photodynamic therapy (PDT) will not be discussed here since many recent reviews on this topic have already appeared.<sup>[32,33]</sup> We note that for certain topic, only a few selected examples are described since this review aims more to highlight principles.

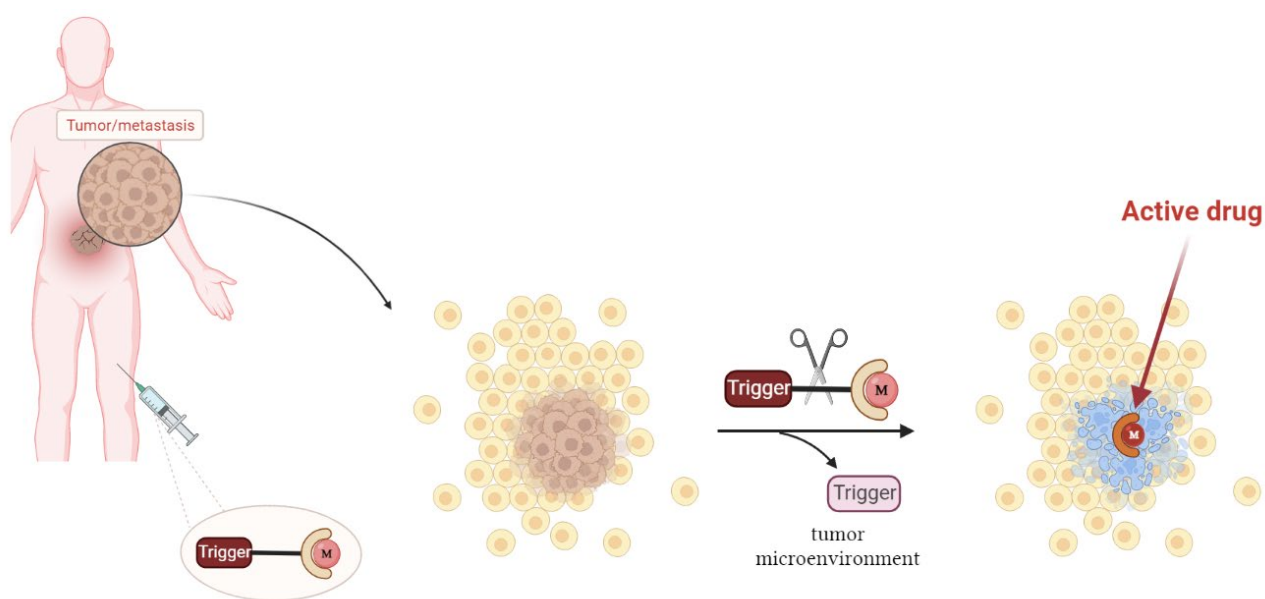


Figure 3. General scheme of selective delivery of metal complexes to the tumor site.

## 2. Enzyme-responsive metal complexes

The design of stimuli-responsive systems that can be activated by an enzyme selectively present in targeted tissues represents a very attractive strategy for the development innovative diagnostic and therapeutic agents. In this approach the active species (e.g., imaging probe, drug, etc.) can be turned on in a catalytic manner, thereby offering a substantial advantage compared to non-catalytic activation processes. Thus, enzyme-responsive metal complexes have been investigated for both imaging and therapeutic purposes.<sup>[23]</sup> In this context, a particular attention has been paid to the targeting of glycosidases, such as  $\beta$ -galactosidase and  $\beta$ -glucuronidase that are overexpressed in some diseased tissues (e.g. tumors),<sup>[34]</sup> and  $\beta$ -lactamase, a bacterial enzyme that can be pre-targeted using DEPT (Directed Enzyme Prodrug Therapy) strategies.<sup>[35]</sup>

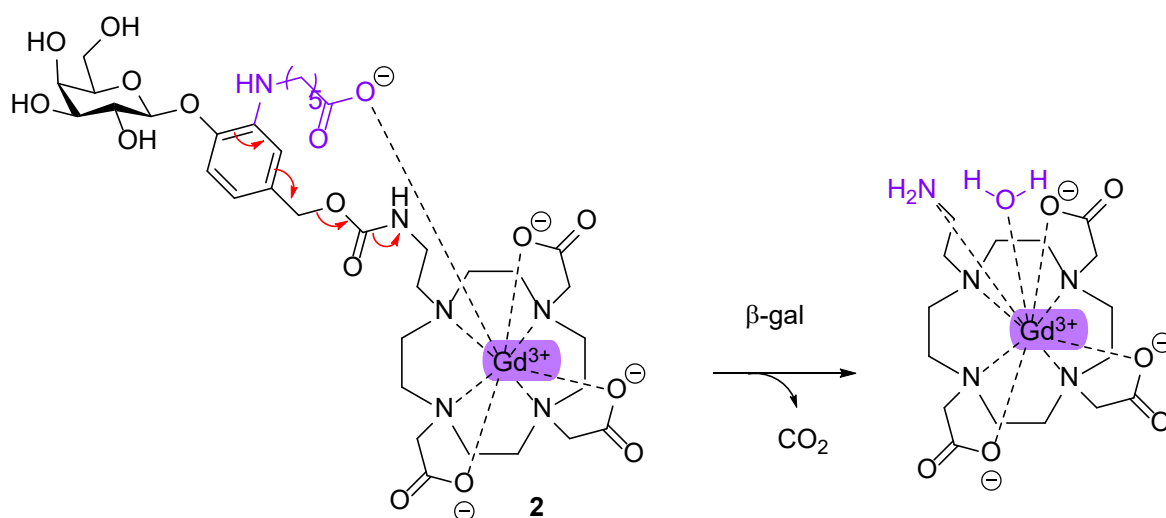
### 2.1. $\beta$ -Galactosidase

#### a. Imaging

Magnetic resonance imaging (MRI) is an alternative to optical microscopy and offers the possibility to study biological structures in 2D or 3D in a non-invasive manner. These images are obtained using the magnetic resonance signal of the nucleus of water's protons. The signal intensity obtained is a function of the water concentration and both the longitudinal relaxation time  $T_1$  and the transverse relaxation time  $T_2$ . The interaction of water molecules with the metal ion leads to a decrease in the  $T_1$  of the complex, resulting in a higher contrast image of the observed object. In 1997, Meade et al. exploited this imaging property by designing the first enzyme-responsive contrast agent.<sup>[36]</sup> They studied the two  $Gd^{3+}$  complexes **1a (EGad)** and **1b (EGadMe)** that included a galactoside on their 9<sup>th</sup> coordination site (Scheme 1). In the presence of  $\beta$ -galactosidase, the glycosidic bond was cleaved, allowing the interaction of water molecules with the paramagnetic ion. This variation in the coordination sphere of the lanthanide decreased the  $T_1$  relaxation time of the complexes resulting in an increased intensity of the

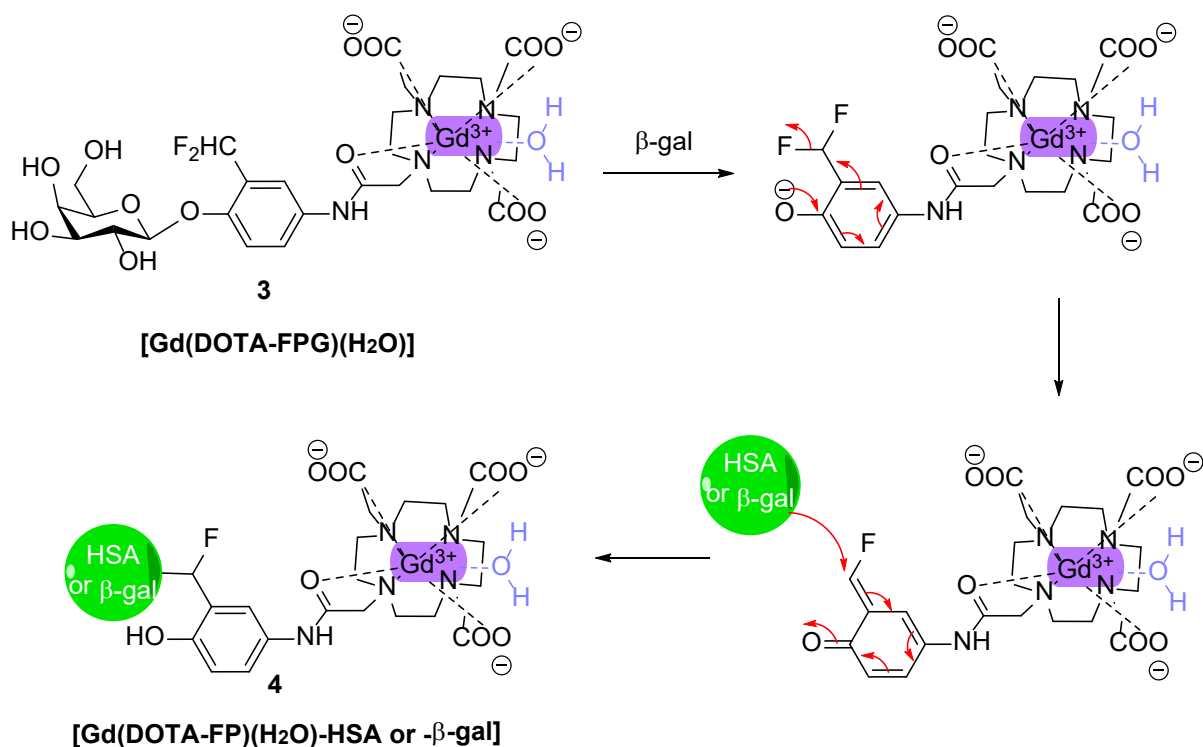


To overcome this drawback, the authors developed the MRI contrast agent **2** including a self-immolative linker that exhibited fast enzymatic kinetics (Scheme 2). The insertion of a pendent carboxylic group on the linker allowed the saturation of the metal coordination sphere, making it inactive.<sup>[39]</sup> Once hydrolyzed by  $\beta$ -gal, the self-immolative linker underwent an electron cascade, releasing the Gd(III) chelate agent and enabling one water molecule to coordinate. The activity of **2** was demonstrated in transgenic mice expressing  $\beta$ -gal.



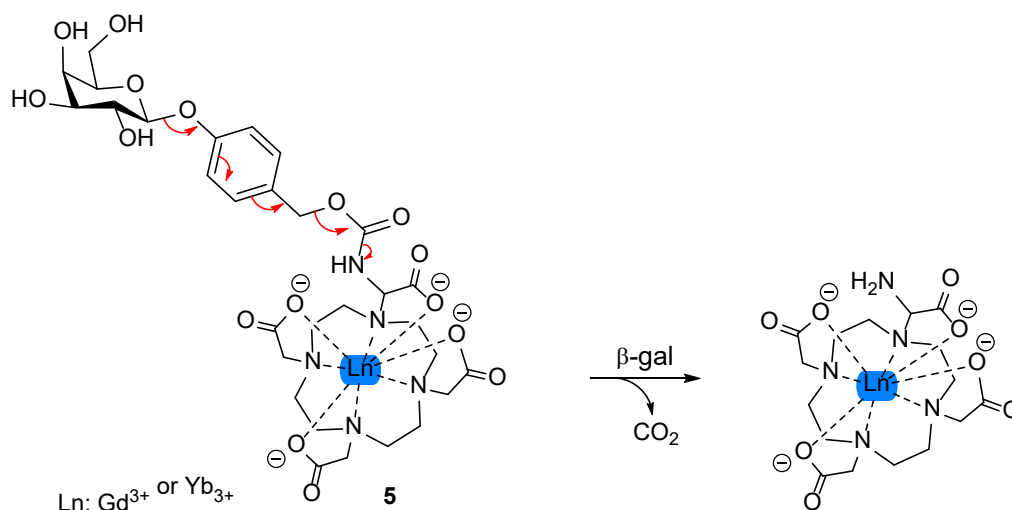
Scheme 2. Mechanism of the MRI contrast agent **2**.

In 2007, Wang et al. reported the complex **3** beared a novel  $\beta$ -galactosidase-sensitive self-immolative linker.<sup>[40]</sup> Once activated, the latter reacted<sup>[40]</sup> with nucleophilic moieties of either human serum albumin (HSA) or  $\beta$ -galactosidase to generate the corresponding bioconjugates **4**, namely **Gd[(DOTA-FP)(H<sub>2</sub>O)]-HSA** and **Gd[(DOTA-FP)(H<sub>2</sub>O)]- $\beta$ -gal** respectively, via the mechanism depicted on Scheme 3. A higher relaxivity and T<sub>1</sub> relaxation time was observed with the HSA-bound chelate agent compared to **Egad 1a**. This new generation of MRI contrast agents showed an enhanced signal intensity in the presence of bio-macromolecules such as  $\beta$ -gal and HSA allowing for the monitoring of enzymatic activity in tumor expressing  $\beta$ -gal.



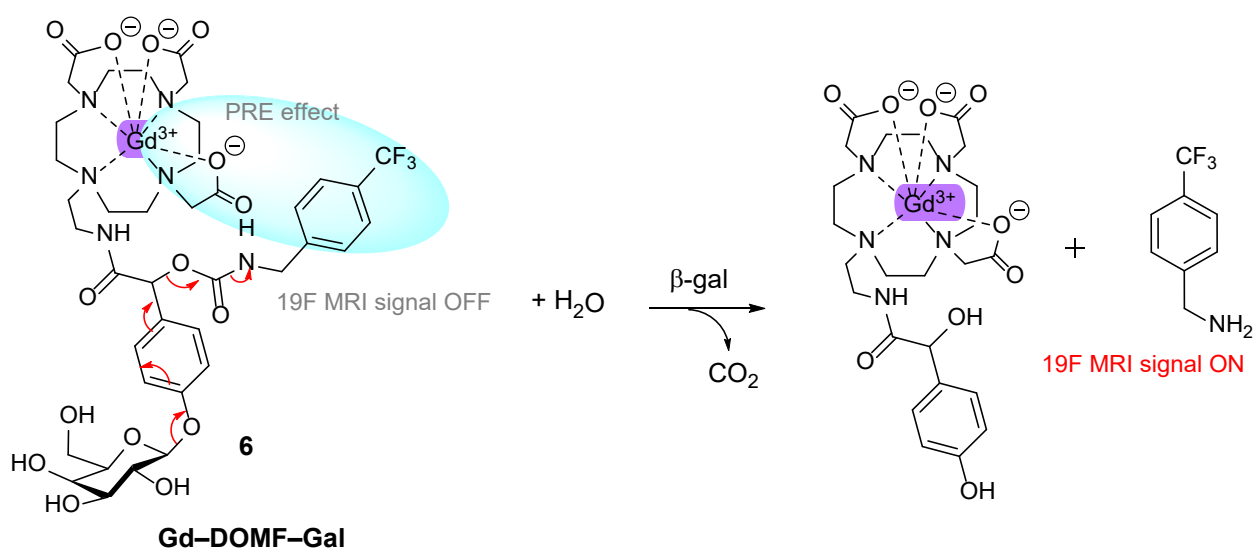
Scheme 3. New generation of Gd-contrast agent: **Gd[(DOTA-FP)(H<sub>2</sub>O)]-HSA or -β-gal**.

In 2008, Chauvin and their co-workers developed enzyme-responsive MRI and PARACEST (Paramagnetic Chemical Exchange Transfer) probes derived from the DOTA ligand.<sup>[41,42]</sup> These off/on probes can overcome the lack of sensitivity of these imaging techniques and target molecules present in low (nanomolar) concentrations. The probes **5** consist of a DOTA ligand encapsulating either Gd<sup>3+</sup> or Yb<sup>3+</sup> and is linked to a β-galactosidase-responsive self-immolative benzylcarbamate moiety (Scheme 4). In the presence of β-galactosidase, the cleavage of the glycosidic bond triggered the self-decomposition of the linker, leading to the release of the corresponding complex. The structural modification of the lanthanide derivative resulted in the modification of the MRI and PARACEST properties of the complexes, therefore allowing the detection of enzymatic activity.



Scheme 4. Lanthanide MRI and PARACEST probes developed by Chauvin et al.

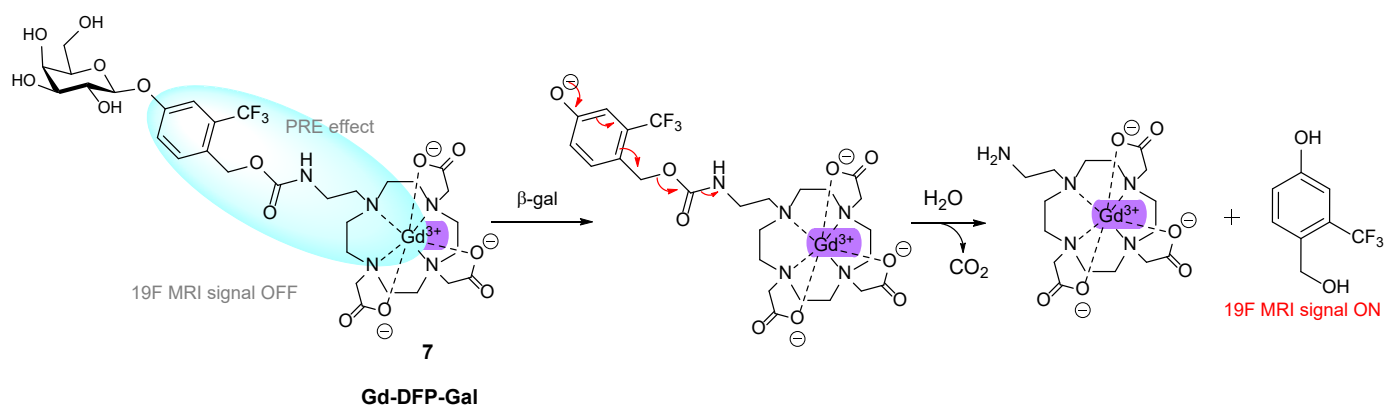
One of the drawbacks of *in vivo* MRI images is the presence of background signals intrinsic from tissues. To overcome this limitation, Engelmann's team developed the bimodal <sup>1</sup>H and <sup>19</sup>F MRI probe **6** (Scheme 5).<sup>[43]</sup> To quench the fluorine signal in the absence of  $\beta$ -gal, the authors exploited the phenomenon of intramolecular shortening of <sup>19</sup>F relaxation times by paramagnetic lanthanide metal ions: the so-called Paramagnetic Relaxation Enhancement (PRE) effect. Enzymatic cleavage of the probe released the fluorine moiety, thereby increasing its relaxation time and consequently the <sup>19</sup>F MRI signal (Scheme 5).



Scheme 5. Visualization of the PRE effect and activation of **6**.

*In vitro* experiments were carried out with **6** (0.96 mM) on melanoma cells expressing  $\beta$ -galactosidase (LacZ/B16) and B16 cells without the targeted enzyme. An acquisition of the  $^{19}\text{F}$  MRI images showed that no  $^{19}\text{F}$  MRI signal could be detected in the samples after incubating B16 cells with probe **6** (either 15 min or 2 h). In contrast, a signal of increasing intensity was observed after incubation of LacZ/B16 cells in the presence of **6**. These results indicated that **6** was efficiently and specifically converted within  $\beta$ -galactosidase-expressing LacZ/B16 cells.

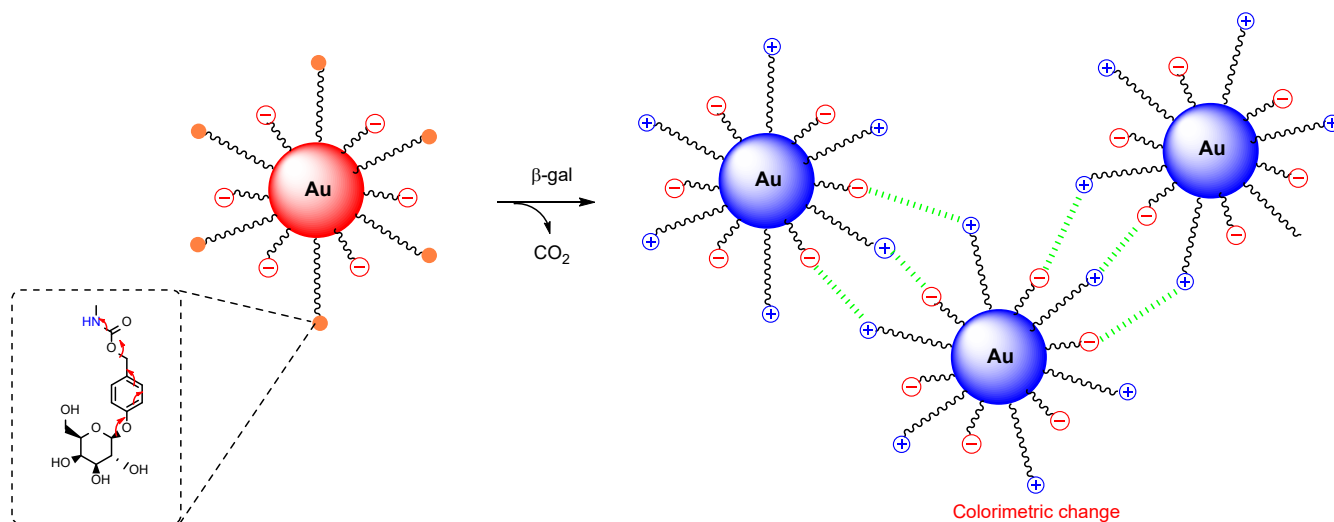
Based on the same principle, Kikuchi et al. developed the new  $^{19}\text{F}$  MRI probe **7** (Scheme 6).<sup>[44]</sup> With this design, the transverse relaxation time  $T_2$  of the trifluoromethyl group was reduced by the PRE effect. As observed by  $^{19}\text{F}$  NMR, enzymatic cleavage of the galactoside increased the  $T_2$  of the trifluoromethyl moiety, therefore enhancing the MRI signal. *In vitro* studies were conducted on HEK293T cells expressing and not expressing  $\beta$ -gal. An increase of the  $^{19}\text{F}$  NMR signal was recorded only in cells expressing  $\beta$ -gal. These results demonstrated the selectivity of the probe **6** for the enzyme and its potential for the detection of the  $\beta$ -galactosidase activity. However, due to hydrophilicity of **6**, the cell membrane needed to be permeabilized for observing the probe activation, which represents a major obstacle for the use of this imaging technology *in vivo*.



Scheme 6. Mechanism of the **Gd-DFP-Gal** probe.



The same authors exploited the properties of gold nanoparticles (AuNPs) to develop new imaging techniques for enzyme detection. First, they designed gold nanoparticles bearing lipoic acid chains with and without glycosidase-responsive ends (Scheme 7).<sup>[45]</sup> In the presence of the corresponding enzyme ( $\beta$ -gal), hydrolysis of the glycosidic bond followed by self-decomposition of the linker led to the release of a positively charged ammonium.



Scheme 7. General mechanism of gold nanoparticles enzyme-responsive probes allowing colorimetric assay for glycosidase activity detection.

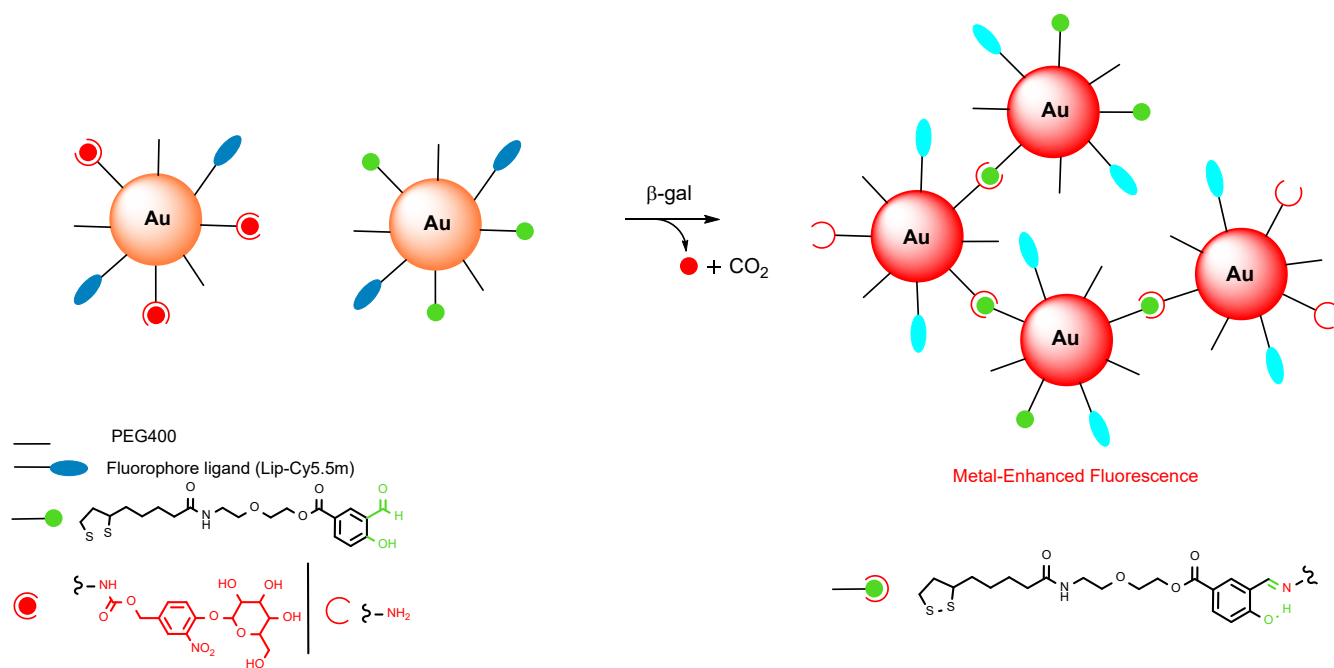
The free ammonium can then interact with anionic lipoate on the neighboring nanoparticle, resulting in electrostatic aggregation. This aggregation induces a colorimetric change from wine red to blue that can be observed with the naked eye. This imaging technique that allows the detection of glycosidase activity in real time presents the advantage of being simple and highly sensitive.

Kikuchi et al. also designed a  $\beta$ -gal metal-enhanced near infrared (NIR) fluorescence sensor based on functionalized gold nanoparticles (AuNPs).<sup>[46]</sup> The aim of this study was also to improve the detection of enzymes *in vivo* for diagnosis purposes.

Metal-enhanced fluorescence (MEF) is due to the localized surface plasmon resonance (LSPR) of noble metals that can increase the fluorescence of a fluorophore when in close proximity

(>5nm). It has been shown that  $\beta$ -gal can shift the LSPR absorption spectrum of the AuNPs from visible to the NIR region.<sup>[45]</sup>

Based on these two properties, the authors synthesized nanoparticles decorated with fluorophore ligands (Lip-Cy5.5m), PEG<sub>400</sub>, and either galactoside or aldehyde ends (Scheme 8).



Scheme 8. Metal-enhanced fluorescence mechanism of functionalized gold nanoparticles.

In the presence of  $\beta$ -gal, the hydrolysis of the galactoside moiety followed by the decomposition of the linker led to the release of an amine that then reacted with the aldehyde of a neighboring particle. Through this fashion, the inter-nanoparticle distance decreased, and the LSPR shifted into the NIR regions. This fluctuation enhanced the electromagnetic resonance coupling and thus the fluorescence.

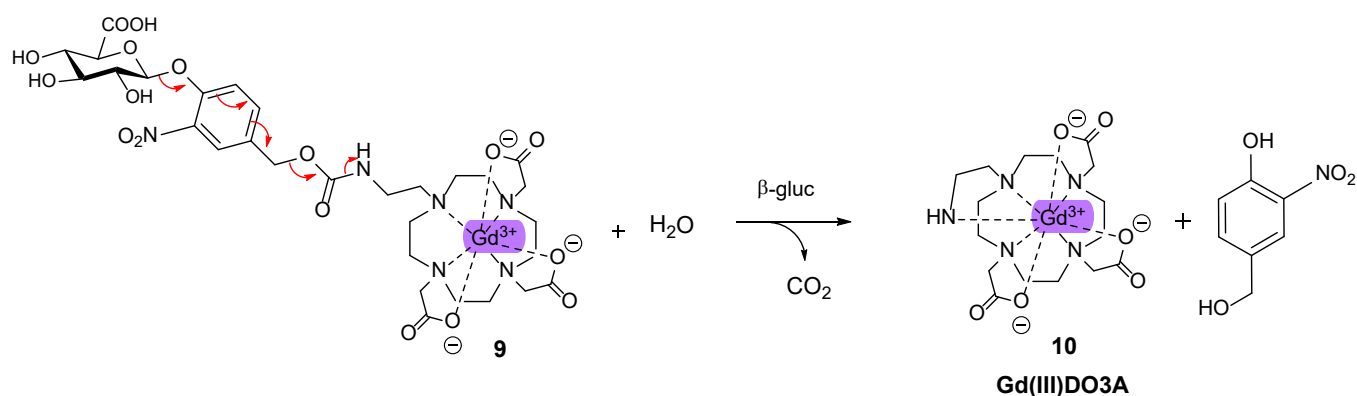
The NIR fluorescence was enhanced by a factor 7.8 showing the potential of such an activatable probe for enzyme detection. This concept can be useful for on-demand imaging techniques such as *in vivo* enzyme detection and early diagnostic imaging.

The use of nanomaterials as drug delivery systems is an approach that has been widely explored. This allows for the masking of the drug activity during its transport until it reaches the diseased tissues, therefore minimizing side effects. However, the unselective drug leakage, a process observed with the vast majority of nano-carriers, represents an important drawback for this targeting strategy both for therapeutic and diagnosis purposes.

## 2.2. $\beta$ -Glucuronidase

### a. Imaging

Inspired by their previous work devoted to the detection of  $\beta$ -gal activity, the Meade group designed the new MRI contrast agent **9** (**Gd(III)DO3A**) including a self-immolative linker sensitive to  $\beta$ -glucuronidase (Scheme 9).<sup>[47]</sup>



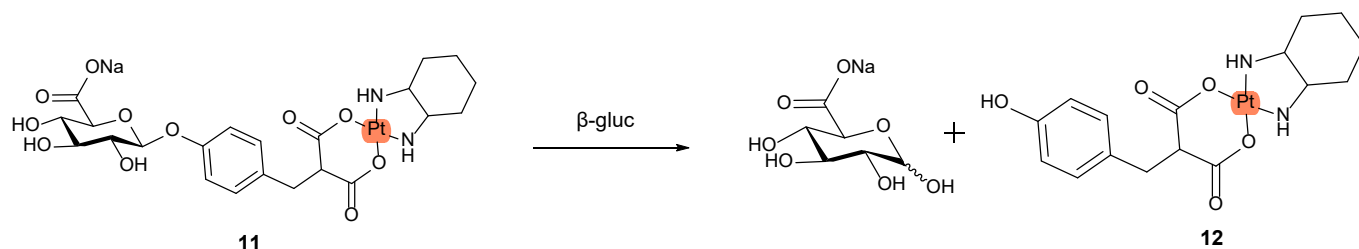
Scheme 9.  $\beta$ -Glucuronidase-catalysed release of **Gd(III)DO3A**.

First, the authors compared the difference in relaxivity properties of **9** and **10** between a competitive extracellular anion mimic solution and human serum. An increase of 240% in relaxivity in the human serum compared to high concentrated anion buffer was observed. Furthermore, the complex **9** was 27% brighter than **10** in the serum, which should be sufficient for *in vivo* imaging. The complex composition of human serum did not allow to ascribe these results to any particular component of the serum. Kinetic studies using bovine liver  $\beta$ -glucuronidase monitored by magnetic resonance correlated the change in  $T_1$  as function of

enzyme incubation time. These experiments demonstrated the efficiency of this contrast agent in a complex biological environment.

### b. Therapy

Platinum-based drugs are chemotherapeutic agents currently used for cancer therapy. However, their poor water solubility as well as their lack of selectivity for tumor cells strongly limit their therapeutic efficacy. In order to overcome these drawbacks, Reedjik et al. developed the hydrophilic glucuronide prodrug **11** designed for the selective delivery of platinum derivatives within malignant tissues (Scheme 10).<sup>[48]</sup>  $\beta$ -Glucuronidase is indeed overexpressed in the microenvironment of almost all solid tumors.<sup>[49]</sup> Thus, selective hydrolysis of the glucuronide **11** should lead to the release of the platinum-based drug **12** in the tumor extracellular space. The latter will then penetrate passively inside surrounding cancer cells to exert its cytotoxic activity.



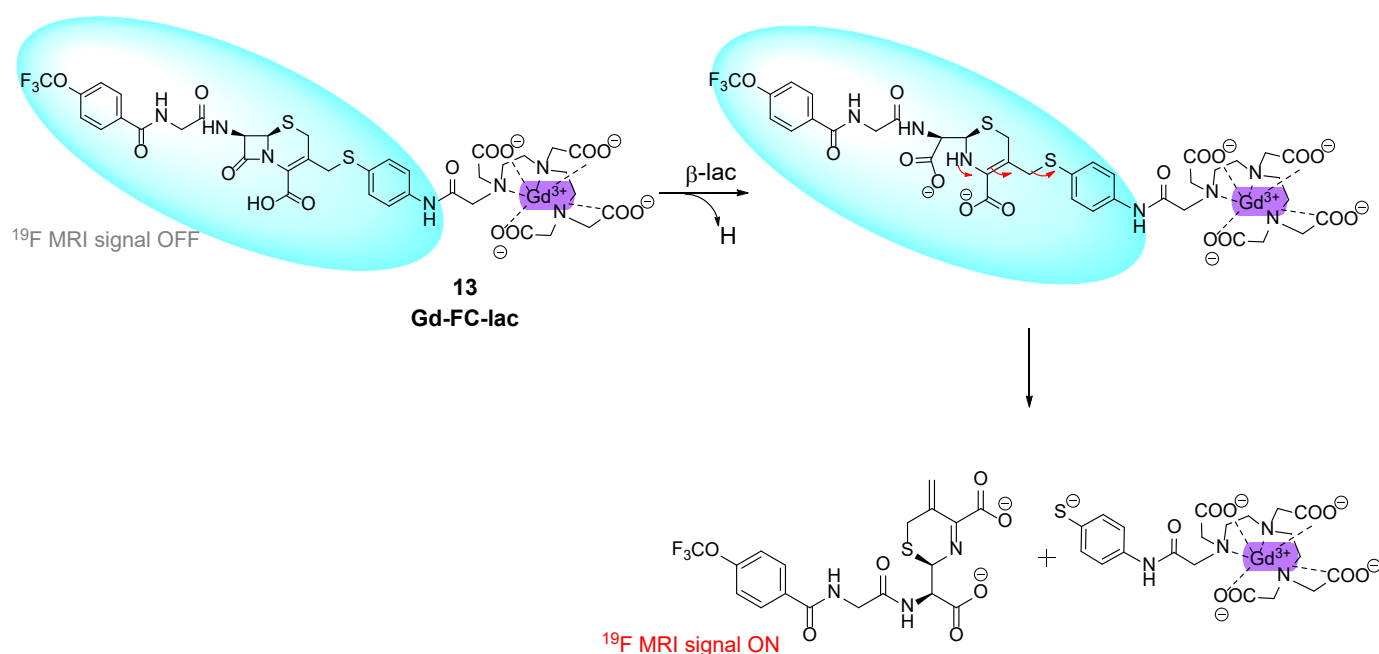
Scheme 10. Hydrolysis of a glucuronide-based Platinum prodrug.

The enzymatic cleavage of prodrug **11** was monitored by <sup>1</sup>H-NMR. The authors demonstrated the relatively fast hydrolysis of the glucuronide to generate the platinum drug. This proof of principle showed for the first time that platinum complexes can be efficiently released upon  $\beta$ -glucuronidase activation, hence highlighting the potential of this approach to improve the selectivity of cancer chemotherapy. Unfortunately, no biological experiment was undertaken to confirm the validity of this targeting strategy.

## 2.3. $\beta$ -Lactamase

### a. Imaging

Kikuchi et al. designed the  $^{19}\text{F}$  MRI probe **13** based on the PRE effect enabling the monitoring of  $\beta$ -lactamase activity expressed on the surface of living cells (Scheme 11).<sup>[50]</sup> The probe was composed of a  $^{19}\text{F}$  group, a cephalosporin moiety, and the  $\text{Gd}^{3+}$  complex. With this design, the large magnetic moment of  $\text{Gd}^{3+}$  reduced the  $T_2$  of the probe and removed the  $^{19}\text{F}$  MRI signal. In the presence of  $\beta$ -lac, the cephalosporin  $\beta$ -lactam ring was hydrolyzed, leading to the release of both the  $\text{Gd}^{3+}$  complex and the  $^{19}\text{F}$  moiety that turn on the  $^{19}\text{F}$  MRI signal.



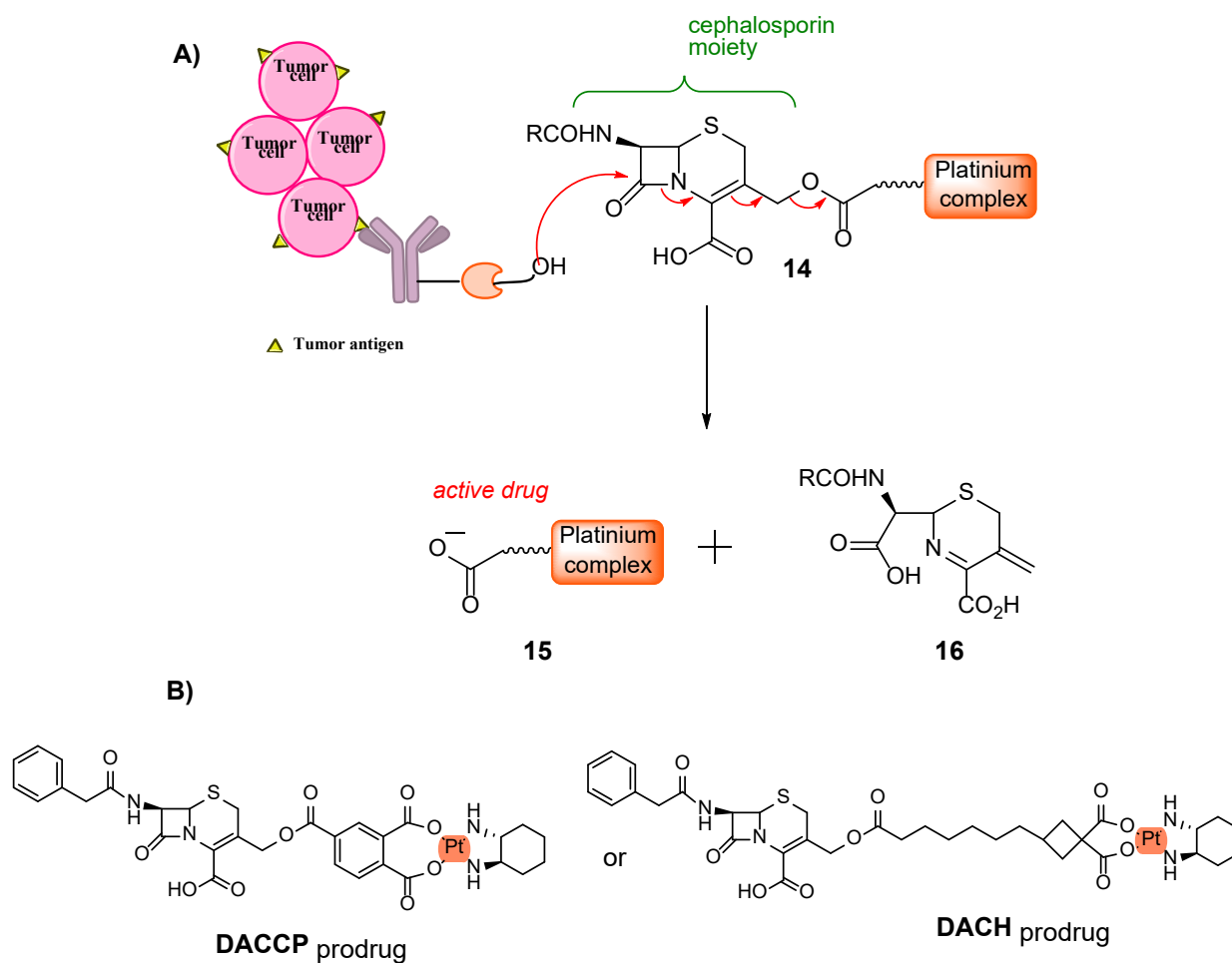
Scheme 11. Structure of the  $\text{Gd-FC-lac}$  probe and its enzymatic hydrolysis.

Using this probe,  $\beta$ -lactamase activity on cell surface was successfully visualized. However, intermolecular PRE was still observed after the enzymatic cleavage, hence lowering the MRI signal intensity.

### b. Therapy

$\beta$ -Lactamase-responsive prodrugs can also be used to release a cytotoxic agent for therapeutic purposes. Thus, with the aim to deliver an anticancer agent selectively at the tumor site,

Hanessian and Wang developed an ADEPT system employing  $\beta$ -lactamase as the triggering enzyme for releasing a platinum complex selectively in malignant tissues (Scheme 12).<sup>[51]</sup> For this purpose, they designed prodrugs **14** bearing different platinum complexes. With this construct, it was anticipated that the enzymatic reaction should lead to the release of the Pt-based drug attached at the 3'-position of cephalosporin residue.



Scheme 12. A). General mechanism of the ADEPT system using  $\beta$ -lactamase and Pt-drug B). Structure of the two platinum prodrugs.

In this study, two potent antitumor agents have been investigated, the 4'-carboxyphthalato (1,2-cyclohexanediamine) platinum (**DACCP**) and the 1,2-diamino cyclohexane (**DACH**) platinum complex.

The  $\beta$ -lactamase hydrolysis of the DACCP derivative was studied by  $^1\text{H}$  NMR in deuterated buffer solutions. These experiments showed the efficient release of the carboplatinium subunit **15** and **16**.

While significant advances have been made in the field of enzyme-responsive metal complexes in past years, some progresses are still needed in order to transfer this approach towards the clinic. Too few experiments have been undertaken *in vivo* so far for estimating the potential of this approach. The next generations of enzyme-responsive metal complexes could be inspired by their organic counterparts that are currently used in humans. For instance, ADCs including an enzyme-sensitive linker enable both the selective accumulation and release of the drug in malignant cells. Thus, enzyme-responsive systems devoted to the delivery of metal complexes could be combined to a targeting warhead like an antibody to enhance their potential as therapeutic or diagnosis agents.

### 3. Other Triggers

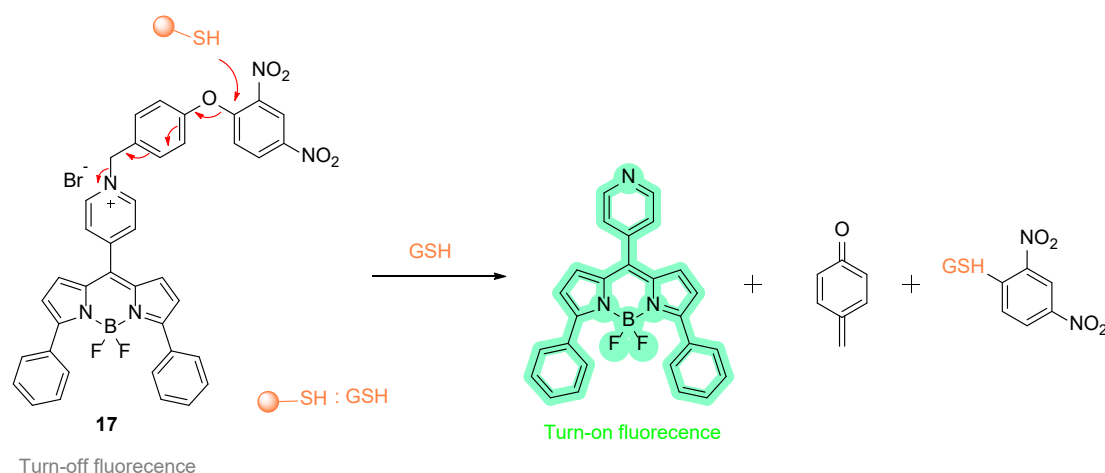
Based on tumor chemical specificities, non-enzymatic stimuli-responsive triggers were also developed. These triggers can respond to exogenous stimuli such as light or endogenous stimuli like ROS or pH variation.

#### 3.1. Chemical Reduction /Redox Activation

##### a. Imaging

Since glutathione (GSH) is present in high concentration in cells of certain disease tissues such as cancer, it has been investigated as an endogenous stimulus for probe activation. GSH can act as a reductive agent or a nucleophile.<sup>[52,53]</sup> Within this framework, Zhao et al. reported the development of the fluorescent probe **17** designed to target mitochondrial GSH in living cells (Scheme 13).<sup>[54]</sup> The probe included a *para*-dinitrophenoxy benzyl pyridinium moiety at the

*meso* position on the BODIPY fluorophore. The pyridinium linker was used as a mitochondrial targeting moiety as well as an electronic sink to turn off the fluorescence of the fluorophore.



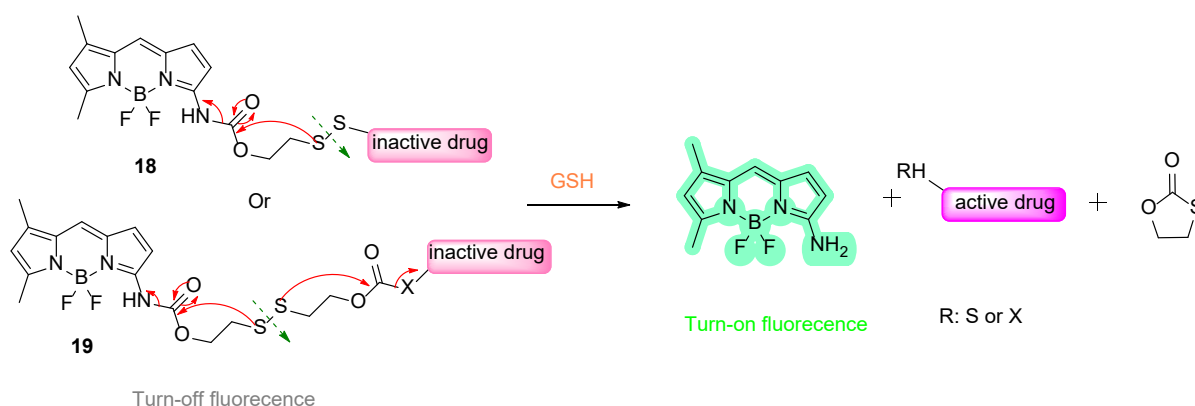
Scheme 13. Mechanism of the BODIPY-GSH probe from Zhao group.

In the first instance, the authors used the 2,4-dinitrophenoxy group for H<sub>2</sub>S detection. However, it turned out that the pyridinium group allowed the selective recognition of GSH instead of H<sub>2</sub>S. A plausible explanation would be the formation of electrostatic interactions between the biothiols and the cationic pyridinium. Therefore, only GSH would reach the reactive site due to the longer chain. Several tests were then carried out to prove the efficiency of this probe. The authors demonstrated that fluorescence increased with the concentration of GSH (up to 32-fold increase with 100 μM of glutathione). In the presence of various biothiol species, GSH demonstrated the fastest response in fluorescence. The detection limit was described at 109 nM of glutathione, hence allowing intracellular imaging. The probe was found to be non-toxic for HeLa cells (cervical cancer cells), and confocal laser scanning microscopic fluorescent imaging showed the localization of the probe in mitochondria.

Hlava's group also developed GSH cleavable conjugates of amino-BODIPY dye to monitor drug release *via* an OFF-ON fluorescent system.<sup>[55]</sup> They conjugated an amino-BODIPY dye to



several 2-phenyl-3-hydroxy-4(1H)-quinolinone (known for their anticancer activity) through the symmetrical **18** or asymmetrical **19** self-immolative linker (Scheme 14).

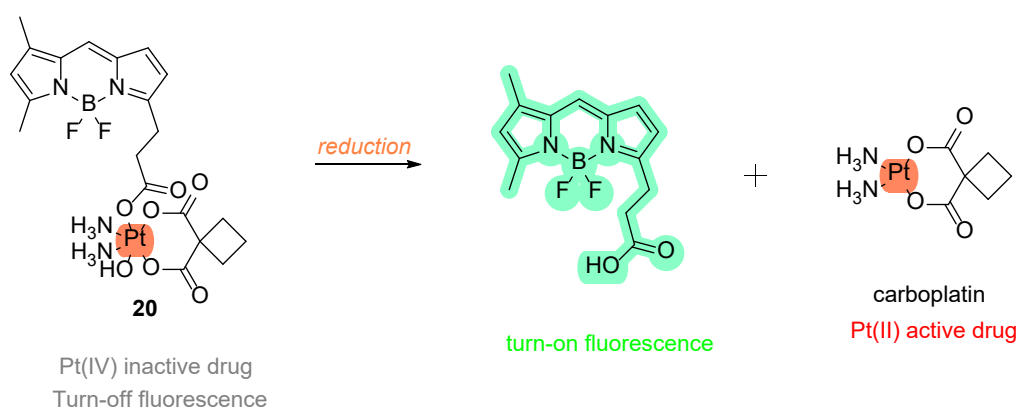


Scheme 14. Fluorescence monitoring system of drug release.

The measured fluorescence spectra showed a lower intensity for the conjugate probe than for the released BODIPY. The cleavage of each conjugate in the presence of GSH was confirmed by HPLC and LC/MS analysis, demonstrating the release of both the BODIPY moiety and the drug. These experiments indicated that measuring the fluorescence of BODIPY reflected the release of the drug. The authors also demonstrated that this probe system can be useful for the delivery of other non-fluorescent drugs (different from quinolinone), highlighting the broad application of this sensing strategy. The efficiency of probe activation was also demonstrated in HeLa cells. However, it was shown that not only glutathione present in biological medium can induce the cleavage but also cysteine. Therefore, this system lacks selectivity and its application for *in vivo* imaging is rather limited.

Pt(IV) complexes have been widely studied as prodrug system delivering active Pt(II) complexes after cellular reduction.<sup>[56–59]</sup> However, in this this review, we only discussed the examples when an active metal complex is released. Recently, Zhu et al. designed the Pt(IV)-

based sensor **20** for investigating the reduction of the platinum (IV) prodrug to platinum (II) in real-time (Scheme 15).<sup>[60]</sup> They demonstrated that the enhanced fluorescence had a linear relationship with the percentage of reduced-Pt and correlated to the cytotoxicity on several cancer cells. However, the sensor concentration and its nearby environment can influence the measurement of the fluorescence intensity. Moreover, no *in vivo* experiment has been performed to investigate the penetration and precision of this sensor on living organism.

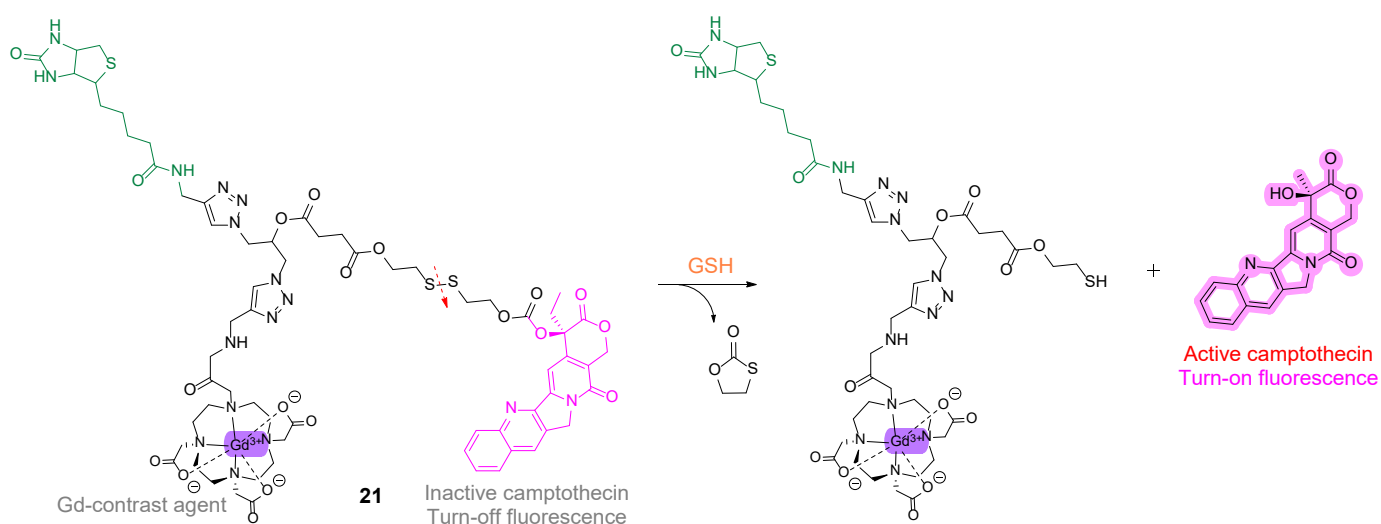


Scheme 15. BODIPY probe for the real-time detection of Pt(II) release.

### b. Therapy

Straddling the line between imaging and therapy, Gao et al. developed the novel prodrug system **21** containing a targeting agent (i.e., biotin), an MRI complex (i.e., Gd-DOTA), an anticancer drug (i.e., camptothecin - CPT) along with a disulfide self-immolative linker (Scheme 16).<sup>[61]</sup> Because of the overexpression of the sodium-dependent multivitamin transporters (SMVT) in some cancer cells, biotin is used as targeting unit to boost the drug efficiency; SMVT is known to transport pantothenic acid (vitamin B5) and biotin.<sup>[62]</sup> Gd-DOTA is a commonly used MRI contrast agent, enabling accurate diagnosis and real-time monitoring. CPT is a powerful antitumor drug, that is very efficient, but it can also bring harmful side effects due to its lack of selectivity for cancer cells. The disulfide linker provides selectivity for the release as the cleavage will take place in the reductive environment present inside tumor cells (i.e., high

concentration of reductive glutathione - GSH). Moreover, the paramagnetic complex would quench the fluorescence of CPT and will turn on after the cleavage. It allows for a complementary approach to monitor drug release.

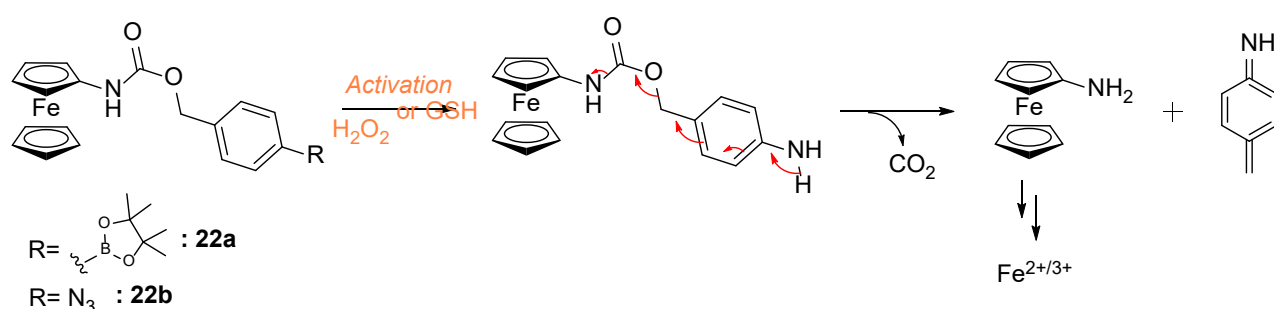


Scheme 16. Mechanism of the release of camptothecin from the biotin-based Gd-contrast agent **5**.

As anticipated, the fluorescence of CPT was increased by 6-fold after cleavage of the disulfide bridge in the presence of GSH, showing the necessity of GSH in the release process. The targeting effect was then demonstrated using two cancer cell lines overexpressing the biotin receptors (BR) — namely HeLa (cervical cancer cells) and A549 (lung epithelial cancer cells). The fluorescence was higher in these cell lines than in non-cancerous cells (i.e. MRC-5 and HL7702). The cellular uptake of **21** was visualized using a MRI scanner and the MR signals increased gradually with the incubation time. IC<sub>50</sub> values of the prodrug in HeLa and A549 cells were lower than the one of CPT only (0.41 and 16.81  $\mu\text{M}$  for the prodrug, respectively compared to 0.79 and 19.82  $\mu\text{M}$  for CPT, respectively). It showed the enhanced cytotoxicity of the prodrug compared to CPT. Additionally, as expected, cytotoxicity against non-cancerous cells was lower for **21** than for CPT, demonstrating better selectivity (>8.00 *versus* 1.97  $\mu\text{M}$  in MRC-5 and 60.40 *versus* 25.51  $\mu\text{M}$  in HL7702 cells). *In vivo* experiments were also conducted

on nude mice bearing A549 tumors. The selectivity of the prodrug was demonstrated by MR signals in the tumor region, and a better therapeutic efficacy of the prodrug compared to free-CPT was revealed by comparing the tumor sizes. Overall, this prodrug system showed great results for both the accurate diagnosis and the precise treatment of tumors. Furthermore, it could be adapted to the targeting of others anticancer drugs.

In 2016, Mokhir and coworkers reported an aminoferrocene prodrug activated by reductive glutathione.<sup>[63]</sup> The system was based on a previous model activated by H<sub>2</sub>O<sub>2</sub> instead of GSH.<sup>[64]</sup> Their first compound **22a** was composed of an aminoferrocene moiety linked to an aryl boronic ester (Scheme 17). The cleavage was induced by H<sub>2</sub>O<sub>2</sub> highly present in cancer cells. To improve the efficiency of prodrug **22a**, the boronic-ester trigger was replaced by an azide residue, which is activated in a reductive environment. The reduction of **22b** produces an amine that can then undergo 1,6-elimination followed by a spontaneous decarboxylation. The two resulting products are the aminoferrocene/Fe salts, which can catalyze the generation of reactive oxygen species (ROS), and the *aza-para*-quinone methide, which alkylates glutathione and hence inhibits the antioxidative system of cells. These two products work in synergy to increase the oxidative stress and cause cell death.

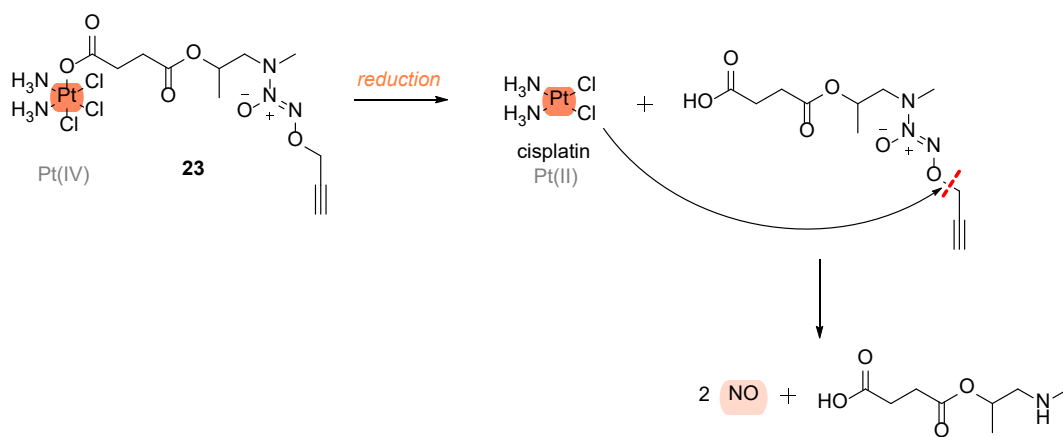


Sscheme 17. Aminoferrocene prodrug **22b** activated by GSH.

The cytotoxicity of compound **22b** was evaluated on the human promyototic leukemia cell line HL-60. The complex was found to be more toxic than the previous drug **22a** bearing the boronic

ester ( $IC_{50}$ :  $27 \pm 4 \mu\text{M}$  versus  $>50 \mu\text{M}$ ). While this prodrug system works *in vitro*, no *in vivo* experiments were conducted, so this system does not provide a full assessment. Furthermore, the compound was not significantly more efficient in hypoxic conditions ( $IC_{50}$ :  $23 \pm 2 \mu\text{M}$  versus  $27 \pm 4 \mu\text{M}$  in normoxic conditions) meaning that the prodrug **22b** is not useful for the treatment of hypoxic tumors.

In 2020, Huang et al. developed a novel strategy relying on a biorthogonal Pt(II) prodrug and a dual theranostic effect.<sup>[65]</sup> Unlike Pt(IV) complexes, Pt(II) complexes are able to catalyze a depargylation reaction, as shown in Scheme 18. *O*-propargylated diazeniumdiolate groups can lead to nitric oxide (NO) cleavage. Knowing that NO has an antiproliferative activity against cancer cells, the authors developed the new kind of biorthogonal prodrug **23** (Scheme 18). For this purpose, a Pt(IV) complex was connected to an *O*-propargyl *N*-methylethanolamine diazeniumdiolate group through a succinic acid moiety.

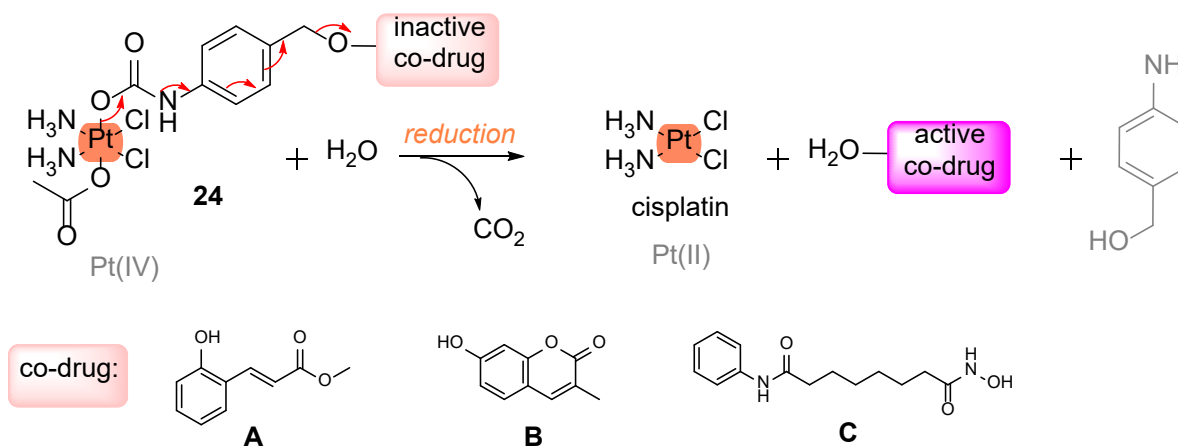


Scheme 18. Mechanism of the dual theranostic effect of prodrug **23**.

Cytoplasmic reductants in cancer cells (e.g., ascorbic acid) reduce the prodrug to form, on one hand, a Pt(II) complex and, on the other hand, a propargyl compound. The Pt(II) complex can then act as theranostic drug and catalyzes the depargylation to liberate NO *in situ*. This system provides synergistic, antiproliferative activity against cancer cells. The prodrug

exhibited a better toxicity ( $IC_{50}$ :  $0.23 \pm 0.01 \mu\text{M}$ ) against human ovarian cancer A2780 cells compared to free cisplatin ( $IC_{50}$ :  $1.08 \pm 0.06 \mu\text{M}$ ) and the Pt(IV) complex alone ( $IC_{50}$ :  $1.69 \pm 0.09 \mu\text{M}$ ). The compound **23** was also found to be less toxic ( $IC_{50}$ :  $119.1 \pm 7.98 \mu\text{M}$ ) against normal epithelial IOSE80 cells than the two free complexes ( $IC_{50}$ :  $8.420 \pm 0.57 \mu\text{M}$  for cisplatin and  $18.47 \pm 1.36 \mu\text{M}$  for the Pt(IV) complex). Finally, the researchers showed cancer cell growth inhibition induced by the prodrug on a zebrafish embryo model, demonstrating its *in vivo* activity. Overall, this new biorthogonal cleavage reaction-based prodrug could be expanded to other active molecules of interest. Moreover, the selectivity against cancer cells, due to the use of a Pt(IV) complex, allows it to overcome the side effects generated by Pt(II)-based drugs.

It is well-known that Pt(II) drugs, especially cisplatin, displays harmful side effects and chemoresistance. Pt(IV) prodrugs are a useful strategy to overcome this limitation. Recently, Ang and their coworkers developed the codrug delivery system **24** using a Pt(IV)-prodrug (Scheme 19).<sup>[66]</sup> For connecting the complex to the bioactive drug, the authors used a 4-aminobenzyl alcohol (4ABA) self-immolative linker, enabling a controlled and traceless codrug release. The intracellular reduction of the platinum complex leads to a decarboxylation and an 1,6-elimination, delivering the active co-drug. Different therapeutic payloads with known anticancer effects have been employed as proof of concept: the methyl trans-2-hydroxycinnamate (MeHC) **A**, the 7-hydroxy-3-methylcoumarin (7-HMC) **B** and the suberoylanilide hydroxamic acid (SAHA) **C**.

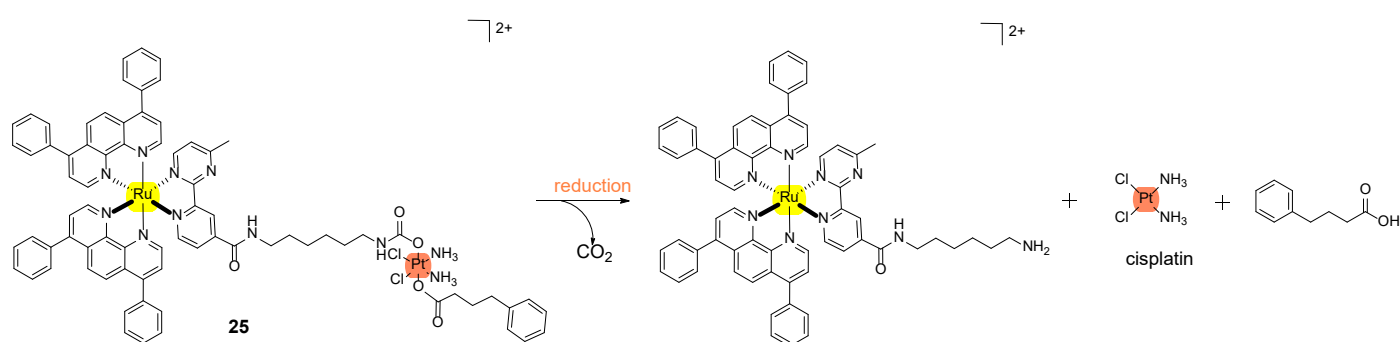


Scheme 19. Illustration of release of the Platinum and the bioactive drug.

Cytotoxicity of the prodrug systems containing **A** or **B** were evaluated on HeLa cervical carcinoma cells. Incubation of the prodrugs showed a better toxicity (IC<sub>50</sub> (**A**): 2.4 ± 0.1 μM and IC<sub>50</sub> (**B**): 5.5 ± 1.0 μM) than each drug alone or when co-injected. For the prodrug system **C**, the antiproliferative efficacy was measured on Pt-sensitive A2780 and Pt-resistant A2780cis ovarian carcinoma cells. Unfortunately, the prodrug was not more cytotoxic than cisplatin against A2780 cells, likely due to its slow 1,6-elimination kinetics. However, the prodrug showed great efficiency against the Pt-resistant A2780 cell line (IC<sub>50</sub> (**C**): 5.2 ± 1.5 μM versus IC<sub>50</sub> (cisplatin): 15.8 ± 2.9 μM). This strategy still needs to be improved and evaluated *in vivo*, but it has already showed promising preliminary results.

In a similar manner, Gasser, Gibson and their co-workers worked on a Ru(II)-Pt(IV) conjugate **25** (Scheme 20). Reduction of the platinum center releases both a Ru(II) polypyridine complex and cisplatin. The Ru(II) complex can act as a photodynamic therapy photosensitizer to generate singlet oxygen upon irradiation either at 480 or even 595 nm. The cytotoxicity of the conjugate was evaluated towards human ovarian carcinoma (A2780), human cisplatin resistant ovarian carcinoma (A2780 cis), and human doxorubicin resistant ovarian carcinoma (A2780 ADR) cell lines in the dark or upon light irradiation. The results were compared with both the Ru(II)

complex alone and with cisplatin. The cytotoxicity in the dark of the conjugate **25** ( $IC_{50} = 0.98 - 01.38 \mu\text{M}$ ) was higher compared to the Ru complex ( $IC_{50} = 15.35 - 18.60 \mu\text{M}$ ) and cisplatin ( $IC_{50} = 4.54 - 19.53$ ). The irradiation drastically improved the cytotoxic profile of **25** providing  $IC_{50}$  values in the nanomolar range ( $IC_{50, 480\text{nm}} = 0.08 - 0.10 \mu\text{M}$ ,  $IC_{50, 595\text{nm}} = 0.16 - 0.19 \mu\text{M}$ ). In contrast, the cytotoxicity of the Ru complex alone was found to be lower on the resistant cell lines A2780 cis and A2780 ADR ( $IC_{50, 480\text{nm}} = 3.41 - 4.67 \mu\text{M}$ ,  $IC_{50, 595 \text{ nm}} = 4.47 - 7.10 \mu\text{M}$ ), clearly showing the beneficial effect of the conjugate **25** to overcome drug resistance.



Scheme 20. Release mechanism of the bioconjugate **25**.

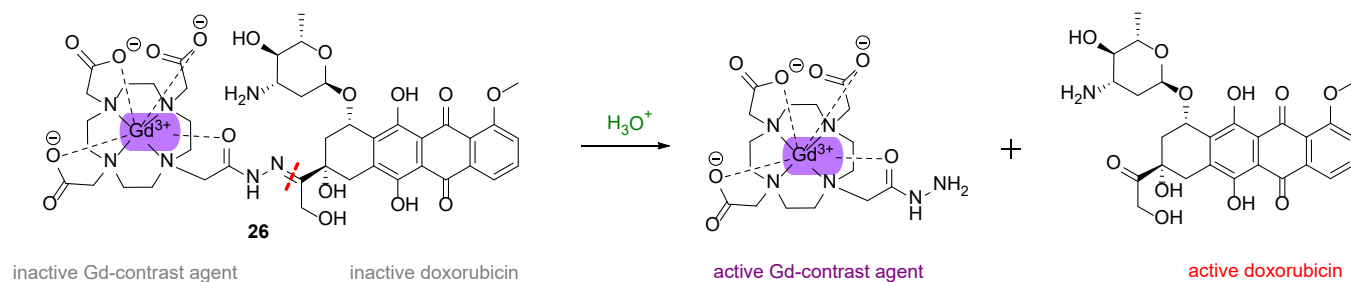
We note that the tremendous work of Hambley and co-workers on the release of active moieties from a Co(III) complex that is reduced to a Co(II) is not discussed in this review since the active species is not the metal-based compound.<sup>[67–69]</sup>

### 3.2. Acidic pH activation

The decrease of extracellular pH in tumors is one of the characteristics allowing for the targeting of malignant cells using a prodrug strategy.<sup>[19,23,70]</sup> In 2006, Meade and their co-workers designed the first complex **26** combining an MRI contrast agent and an anticancer drug (doxorubicin) via an acid-labile hydrazone linker (Scheme 21).<sup>[71]</sup> Doxorubicin is a well-known anticancer agent exhibiting high efficiency, but it also has toxic side-effects. Few doxorubicin prodrugs using acid-labile linkers have been reported to date.<sup>[72]</sup> The linker in **26** is cleaved by the lysosomal acidic pH, allowing intracellular drug release. In previous systems, this release was measured indirectly by high-performance liquid chromatography and cytotoxicity studies.



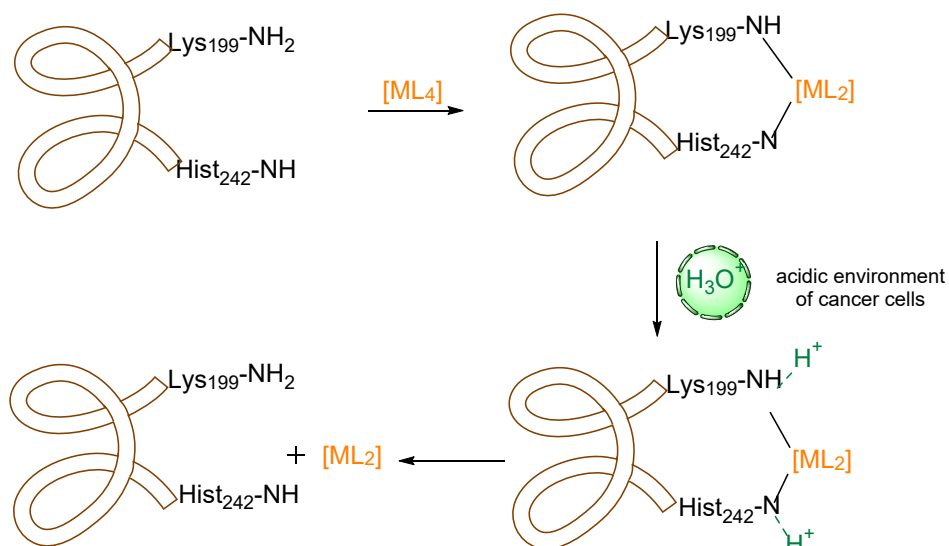
To overcome this limitation, Meade and their co-workers designed the first prodrug-procontrast agent **26** (i.e., a doxorubicin-Gd(III) conjugate shown in Scheme 21).<sup>[73]</sup> The contrast agent is called procontrast agent because it is inactive before the drug release. When exposed to low pH, the prodrug releases the doxorubicin, and the MRI contrast agent undergoes a change in relaxivity, allowing for imaging.



Scheme 21. Acidic-mediated release of the Gd-contrast agent and doxorubicin.

The hydrolytic stability of the compound at pH 7.4 and 4.5 was assessed by relaxometry at 37°C. A decrease in relaxivity was observed at pH 4.5. 90% of doxorubicin was released within 16h, as observed by reversed-phase high-performance liquid chromatography. This lead compound opens up the door for a new class of prodrugs.<sup>[74]</sup> Improvements are still needed for allowing detection at lower concentrations. For this purpose, relaxivities must be improved. *In vivo* experiments have not been reported yet.

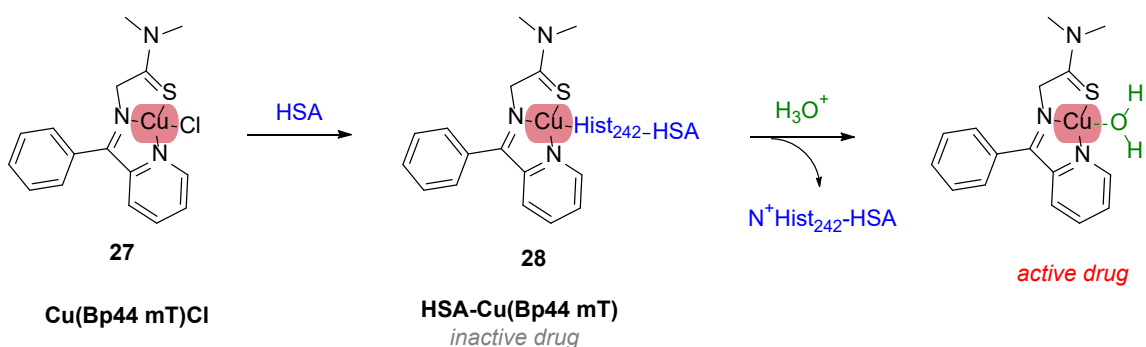
Recently, HSA-based drug delivery systems tethered to a metallodrug have emerged.<sup>[75–81]</sup> The large hydrophobic cavity in the HSA IIA subdomain is constituted of two N-donor residues, namely Lys199 and His242, which can be linked to a metal complex. In the acidic tumor microenvironment, the N-donor residues become protonated, which decreases their ability to coordinate with the metal. Through this fashion, the metallodrug is released (Scheme 22).<sup>[82]</sup>



Scheme 22. General release mechanism of HSA-based metal drugs.

This concept was then extensively exploited by Yang, Liang and their co-workers using several Cu-based drugs. The authors played on different parameters (e.g., using two copper centers,<sup>[83]</sup> replacing the ligand,<sup>[80,81]</sup> modifying the leaving groups,<sup>[79]</sup> adding a folate moiety for targeting,<sup>[84]</sup> creating nanoparticles, etc.<sup>[85]</sup>) to improve the efficiency, selectivity and solubility of the drug.

The best Cu-based prodrug developed so far is the HSA complex **28** (Scheme 23).<sup>[81]</sup> Its cytotoxicity was evaluated *in vitro* on A549 cells (adenocarcinoma human alveolar basal epithelial cells) and *in vivo* on A549 tumor xenograft implanted in nude mice. The prodrug was about 5-fold more toxic than the complex alone **26** [IC<sub>50</sub> (**28**): 0.03 ± 0.01 μM *versus* IC<sub>50</sub> (**27**): 0.15 ± 0.01 μM]. *In vivo* experiments showed a decrease by half of the tumor weight after treatment with the HSA-prodrug **28** compared to a decrease of about 30% for **27**. The authors also investigated the Cu(II) prodrug **27** release from the HSA carrier at pH 4.7 and 7.4 and demonstrated that 5% of **27** was released at pH 7.4 within 48 h versus 80% at pH 4.7.



Scheme 23: Formation of the **HSA-Cu(Bp44 mT)** prodrug followed by the release in acidic environment of the metal-based drug.

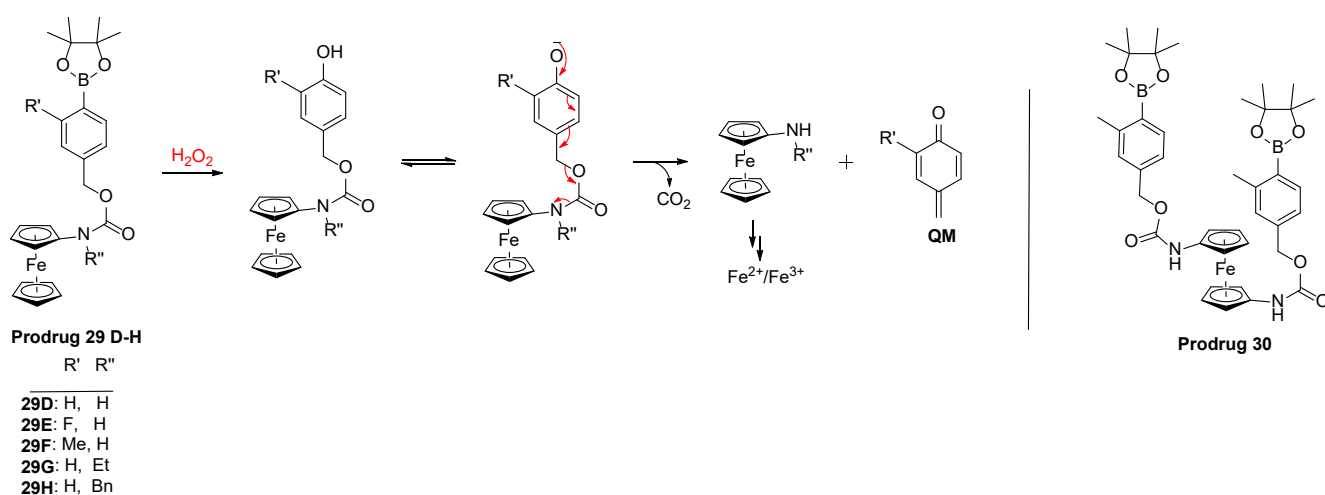
A plausible explanation for these promising results is the better cellular uptake and selectivity of release in cancer cells of the prodrug **28** compared to the complex **27** due to the presence of the HSA moiety. This concept was shown to be effective with copper complexes and more recently with iron complexes.<sup>[78]</sup> Other metal centers remain to be evaluated. Despite these promising results, to the best of our knowledge, no pH-responsive prodrugs entered into clinical trial for now.<sup>[86]</sup>

### 3.3. Activation by the high production of ROS

Most cancer cells exhibit enhanced reactive oxygen species (ROS) production, including  $^1\text{O}_2$ ,  $\text{O}_2^-$ ,  $\text{HO}^\cdot$  and  $\text{H}_2\text{O}_2$  (i.e.,  $[\text{H}_2\text{O}_2]_{\text{cancer cells}}$ : 10-100  $\mu\text{M}$ ;  $[\text{H}_2\text{O}_2]_{\text{normal cells}}$ : 0.001-0.7  $\mu\text{M}$ ). This characteristic makes cancer cells highly vulnerable to oxidative stress. Mokhir et al. decided to use this feature to design ROS-sensitive prodrugs. Their system is based on an aminoferrocene drug linked to a pinacol ester of 4-(hydroxymethyl)phenylboronic acid via a carbamate linker, as shown in Scheme 24. Under ROS exposure, the B-C bond is cleaved to form a phenol, which, under aqueous conditions, undergoes spontaneous 1,6-elimination to release the ferrocene derivative and a *p*-quinone methide (QM). Boronic acid is also formed, which is non-toxic. QM is a glutathione scavenger, thus inhibiting antioxidative system of cells. The ferrocene moiety

acts as a catalyst for ROS generation. This prodrug system leads to a double antiproliferative action in cancer cells.

Mokhir and their coworkers explored this system with different substituents R' and R'' on the prodrug (Scheme 24) to modulate the cell-membrane permeability and thus cell cytotoxicity on human promyelocytic leukemia (HL-60).<sup>[87]</sup> The best compound was **29H** with an IC<sub>50</sub>: 9 ± 2 μM compare to **28D-G** with an IC<sub>50</sub> between 24 and 55 μM. In contrast, the ferrocene alone was not toxic (IC<sub>50</sub> > 200 μM). Importantly, **29H** exhibited no toxicity (up to 100 μM) towards nonmalignant fibroblasts.

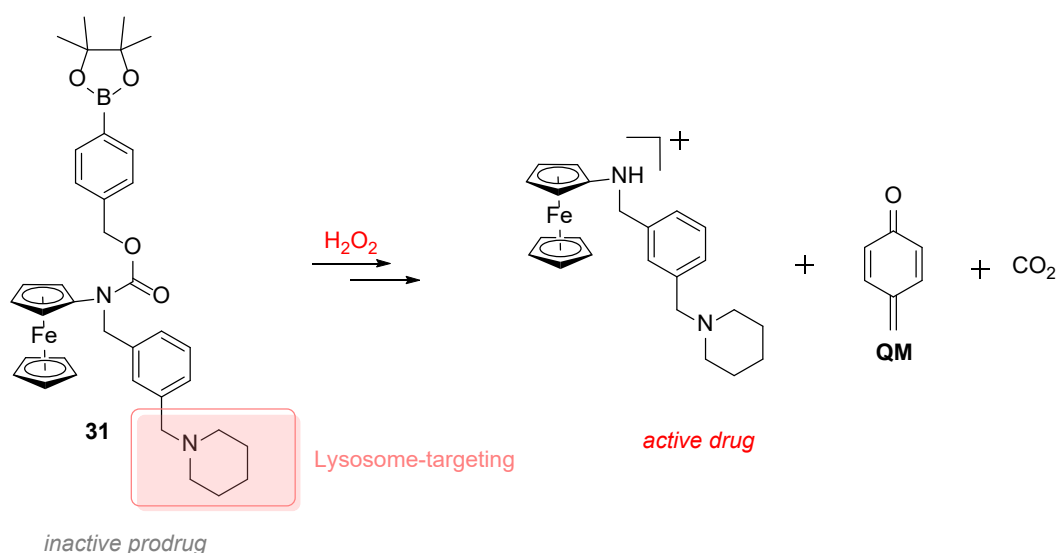


Scheme 24. Structures and mechanisms of ROS-sensitive ferrocene prodrugs.

After this first discovery, this research group attempted to improve their prodrug system. To do so, in 2013, they found out that **30** (Scheme 24) had an IC<sub>50</sub> of 1.4 ± 2.1 μM on primary chronic lymphocytic leukemia (CLL) cells, which is similar to **29H** (IC<sub>50</sub> of 1.5 1 μM).<sup>[64]</sup> In 2015, they tested **29H**, which was the best compound found at this time, against two prostate cancer cell lines, namely LnCaP and DU-145. Interesting IC<sub>50</sub> values were found for **29H** (IC<sub>50</sub> (LnCaP) = 11-17 μM ; IC<sub>50</sub> (DU-145) = 18-27 μM) compared to the *N*-unsubstituted prodrug **29D**, which was not toxic towards both cell lines (IC<sub>50</sub> > 50 μM). These values correlated with an increase of intracellular ROS amount by 11-18 fold compared to that observed with the ferrocene

alone.<sup>[88]</sup> Preliminary *in vivo* studies also showed a strong concentration-dependent growth inhibition of the tumor after treatment with **29H**.

However, at low micromolar concentration of the prodrugs, the activation by ROS is not efficient enough. Since lysosomes contain a higher concentration of ROS than the cytoplasm, Mokhir et al. designed prodrug analogues of **29H** containing an alkylated piperidine fragment to target the lysosomes (Scheme 25).<sup>[89]</sup> The acidic environment of the lysosome protonates the piperidine, leading to the trapping of the prodrug in this organelle. The authors studied the toxicity of **31** (Scheme 25) against human blood cancer cell lines (i.e., BL-2 and Jurkat-cells). **31** showed better activity than **29H** ( $IC_{50}(\mathbf{31}) = 3.5 \pm 0.9$  versus  $IC_{50}(\mathbf{29H}) 26 \pm 5 \mu\text{M}$  on BL-2 cells and  $IC_{50}(\mathbf{31}) = 7.2 \pm 0.1$  versus  $IC_{50}(\mathbf{29H}) 44 \pm 2 \mu\text{M}$  on Jurkat cells) and induced a 7-35 fold higher oxidative stress in BL-2 cells than **29H**. The prodrug was then evaluated on a murine Nemeth–Kellner lymphoma model and was shown to exhibit a higher tumor growth inhibition by 2.3 times compared to the control (i.e., DMSO).



Scheme 25. Illustration of the lysosome-targeting ROS-responsive prodrug system.

ROS generation is also more important in the mitochondria than in the cytoplasm. That is the reason why Mokhir's team explored a hybrid of **29H** that accumulates in mitochondria after

ROS activation in cells.<sup>[90]</sup> Since the first model envisioned was not very efficient, the authors designed new prodrugs **32** and **33** (Figure 4), which first accumulate in mitochondria before being activated.<sup>[91]</sup> Unfortunately, ROS produced in mitochondria were shown to be insufficient for activation of the ROS-responsive prodrugs.

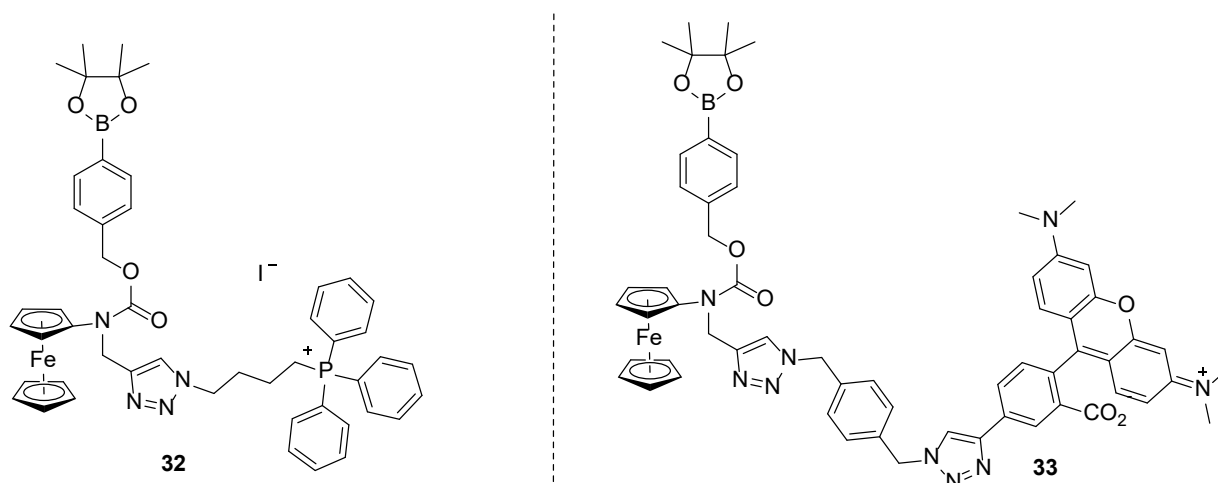
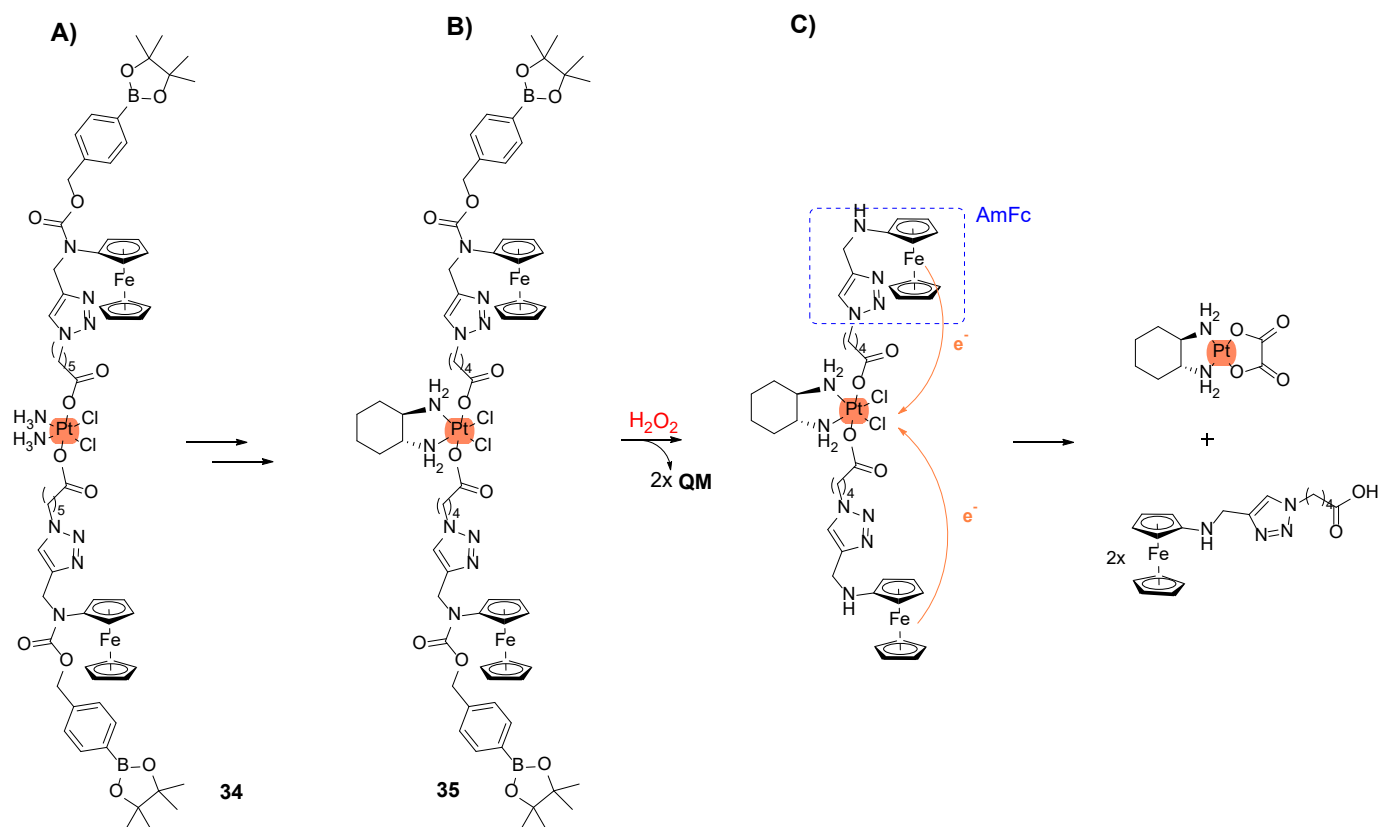


Figure 4. Structures of prodrugs **32** and **33**.

In parallel, Mokhir and their co-workers also developed Pt(IV) prodrugs based on this ROS-activated prodrug system. Pt(IV) prodrugs are known to overcome the usual side effects of Pt(II) drugs and to show activity against cisplatin-resistant cancer cells. Unfortunately, extracellular reduction of Pt(IV) prodrugs decreased their anticancer activity. To overcome this limitation, the group designed a Pt(IV)-based prodrug **34** containing an aminoferrocene (AmFc) moiety, which can be activated by ROS thanks to the boronic pinacol ester fragment (Scheme 26). The first model described in 2017 used a cisplatin-Pt(IV) complex and showed nice preliminary results ( $IC_{50}(\mathbf{34}) = 2.5 \pm 0.5 \mu\text{M}$  on human carcinoma A2780 cells and  $IC_{50}(\mathbf{34}) = 6 \pm 1 \mu\text{M}$  towards cisplatin-resistant cell line A2780cis).<sup>[92]</sup> Yet, the activity was not better than cisplatin alone ( $IC_{50}(\text{cisplatin}) 2.1 \mu\text{M}$ ). To improve the model, the authors used an-oxaliplatin based Pt(IV) prodrug instead of a cisplatin one (compound **35** in Scheme 26) and shortened the linker by one methylene group between the AmFc moiety and the Pt(IV) to improve the

intramolecular  $e^-$ -transfer (Scheme 26).<sup>[93]</sup> The prodrug **35** showed a better cytotoxicity than **34** on A2780 cells ( $IC_{50}(\mathbf{35}) = 0.4 \pm 0.1 \mu\text{M}$ ) and against A2780cis cells ( $IC_{50}(\mathbf{35}) = 0.7 \pm 0.2 \mu\text{M}$ ) and was found to be not cytotoxic for normal cells. *In vivo* experiments still need to be conducted to assess the full potential of this compound.

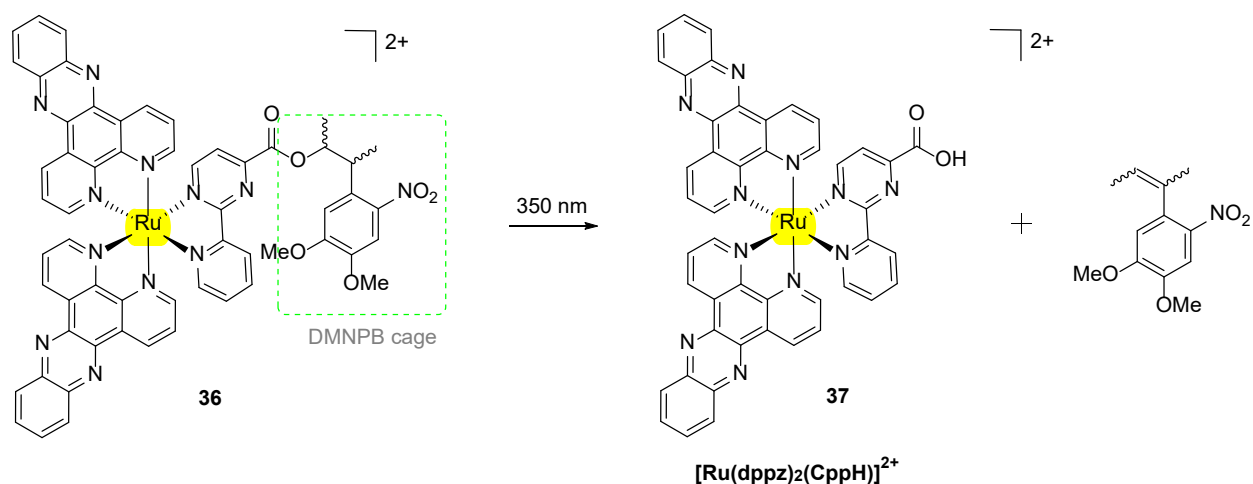


Scheme 26. Structures of compounds A) **34** and B) **35**. C) Release mechanism in the presence of ROS of **35**.

### 3.4. Photo-deprotection

The use of a light-triggered prodrug strategy is an effective approach to provide temporal and spatial control of the drug release. Unlike photodynamic therapy (PDT), this light-mediated strategy does not rely on the presence of oxygen in the tumor, allowing hypoxic solid tumors to be targeted. This strategy is based on a photoremovable moiety, which releases the active drug upon light irradiation. This technique was widely used to release organic compounds, sometimes using metal-based photo-cages like Ru(II) polypyridyl complexes – we note that we

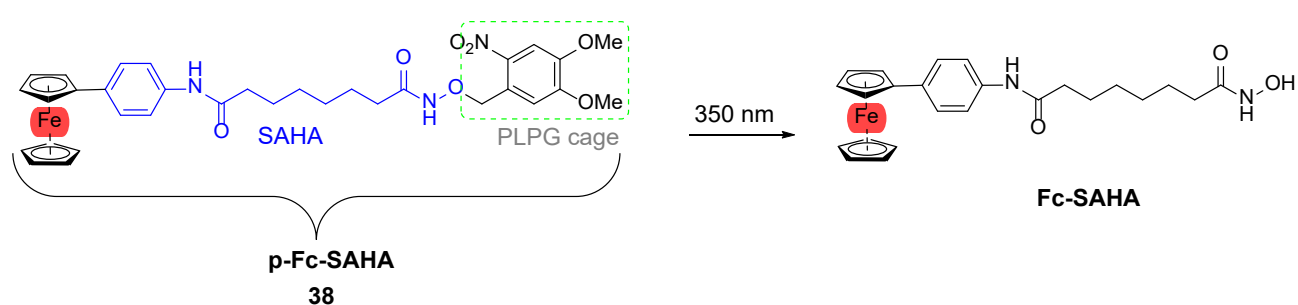
do not discuss in this article the use of metal complexes in photo-activated chemotherapy (PACT) since this topic has been recently reviewed and since we focus on the release of active metal complexes.<sup>[94,95]</sup> To the best of our knowledge, it was only in 2013 that the first metal complex, namely an inert Ru(II) complex, was photo-released upon light irradiation.<sup>[96]</sup> Indeed, Gasser et al. first developed a Ru(II) polypyridyl complex  $[\text{Ru}(\text{dppz})_2(\text{CppH})]^{2+}$ , which was found to be extremely cytotoxic on different cell lines.<sup>[97]</sup> Knowing that the carboxylate function on the pyrimidine ring was essential for the cytotoxic activity, the authors hide it with a photocleavable moiety (i.e., DMNPB: 3-(4,5-dimethoxy-2-nitrophenyl)-2-butyl) to form **36** (Scheme 27). The cytotoxic evaluation was conducted on cervical cancer (Hela), bone cancer (U2OS), and non-cancerous lung fibroblast (MRC-5) in the dark and under 350 nm light irradiation ( $2.58 \text{ J}\cdot\text{cm}^{-2}$ ). In the dark, the prodrug **36** was found, as anticipated, to be not toxic, while **37** was  $[\text{IC}_{50}(\mathbf{36}) > 100 \text{ }\mu\text{M}]$  compared to  $[\text{IC}_{50}(\mathbf{37}) = 16\text{-}30.5 \text{ }\mu\text{M}]$  in Hela and U2OS cells]. As expected, upon light irradiation, **36** showed promising cytotoxicity  $[\text{IC}_{50}(\mathbf{36}) = 17.0 \pm 0.8 \text{ }\mu\text{M}]$  against Hela cells and  $[\text{IC}_{50}(\mathbf{36}) = 17.2 \pm 3.8 \text{ }\mu\text{M}]$  on U2OS cells]. Notably, **37** alone was found to be more cytotoxic upon light irradiation than the prodrug **36**  $[\text{IC}_{50}(\mathbf{37}) = 5.9 \pm 1.7 \text{ }\mu\text{M}]$  towards Hela cells and  $[\text{IC}_{50}(\mathbf{37}) = 13.5 \pm 2.1 \text{ }\mu\text{M}]$  on U2OS cells], possibly due singlet oxygen production.



Scheme 27. Structure of **36** and its photodeprotection to form the cytotoxic  $[\text{Ru}(\text{dppz})_2(\text{CppH})]^{2+}$ .



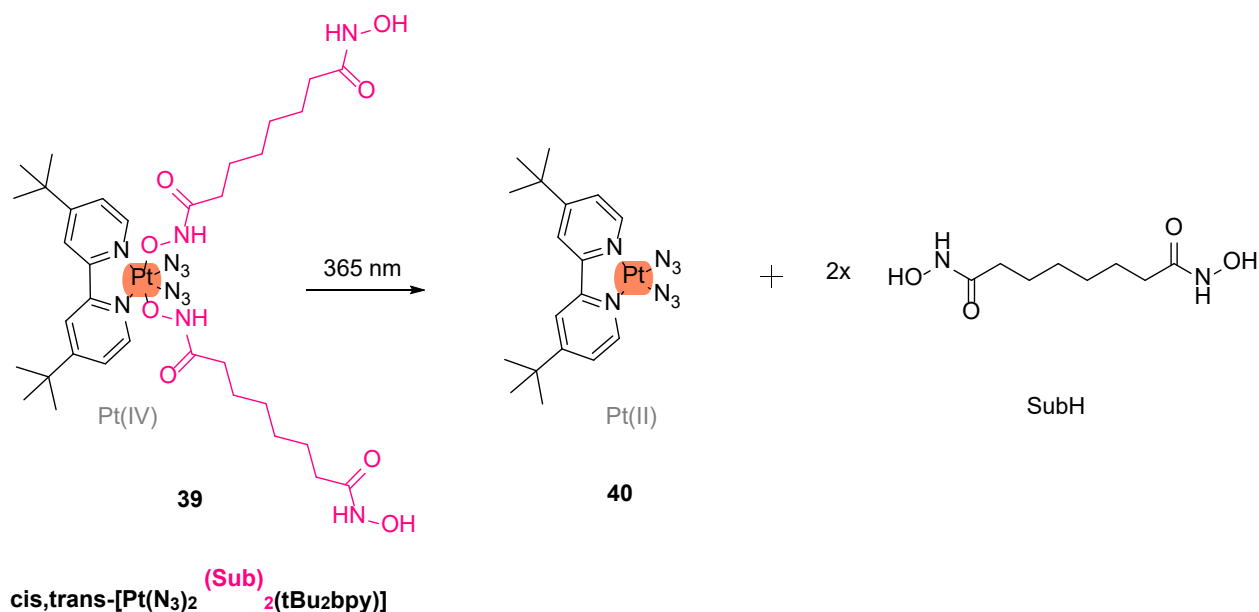
The same group then investigated this prodrug strategy on ruthenium and rhenium complexes conjugated to targeting peptides, such as bombesin, to boost the cellular uptake by malignant tissues and add cellular specificity.<sup>[98,99]</sup> The Re compound presented better activity than the Ru complex, but optimization are still required, especially for the choice of the wavelength to allow deeper tissue penetration for *in vivo* experiments. In 2016, the same team developed the first light-activable organometallic histone deacetylase (HDACs) inhibitor.<sup>[100]</sup> HDAC is a key enzyme in cancer as well as metabolic syndromes and neurodegenerative diseases, making HDAC inhibitors very attractive. SAHA (suberoylanilidehydroxamic acid) was approved to treat cutaneous T-cell lymphoma (CTCL), although it presents severe side effects and low efficiency on solid tumors. This is the reason why the authors designed a photo-labile HDAC inhibitor **38** combined with a ferrocene, on which the hydroxamic acid function was photocaged with a PLPG (i.e., 1-(bromomethyl)-4,5-dimethoxy-2-nitro-benzene) moiety (Scheme 28). HDACs inhibition was evaluated on HDAC1, HDAC2, and HDAC6 enzymes in the dark and upon UV-A irradiation (350 nm; 2.79 J.cm<sup>-2</sup>). IC<sub>50</sub> values determined upon light irradiation were similar to SAHA and Fc-SAHA.



Scheme 28. light-activatable histone deacetylase inhibitor **p-Fc-SAHA**.

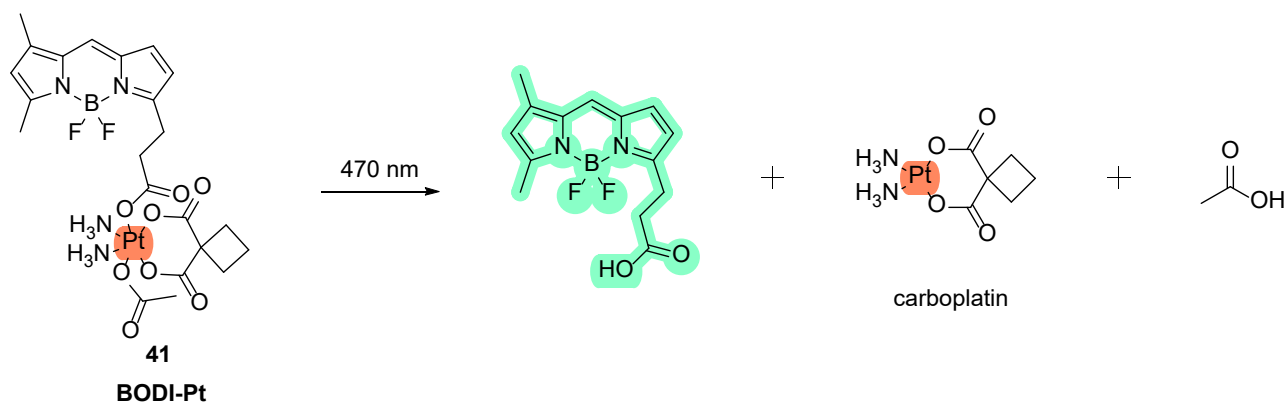
This first evaluation opened the field to other photoactivable HDACs inhibitors. Braber et al. developed a photoactivable Pt(IV) complex **39** conjugated to an HDAC inhibitor (SubH: suberoyl-bis-hydroxamic acid) (Scheme 29).<sup>[101]</sup> The prodrug **39** was then evaluated on human

ovarian cell lines A2780 and resistant cell lines A2780cisR. It showed high toxicity values after irradiation at 365 nm ( $IC_{50}(\mathbf{39}) = 3.3 \pm 0.3 \mu\text{M}$  versus  $IC_{50}(\text{cisplatin}) = 18 \pm 1 \mu\text{M}$  on A2780 cells and  $IC_{50}(\mathbf{39}) = 3.9 \pm 0.5 \mu\text{M}$  versus  $IC_{50}(\text{cisplatin}) = 45 \pm 2 \mu\text{M}$  against A2780cisR cells). These promising results need to be further explored, notably with *in vivo* experiments.



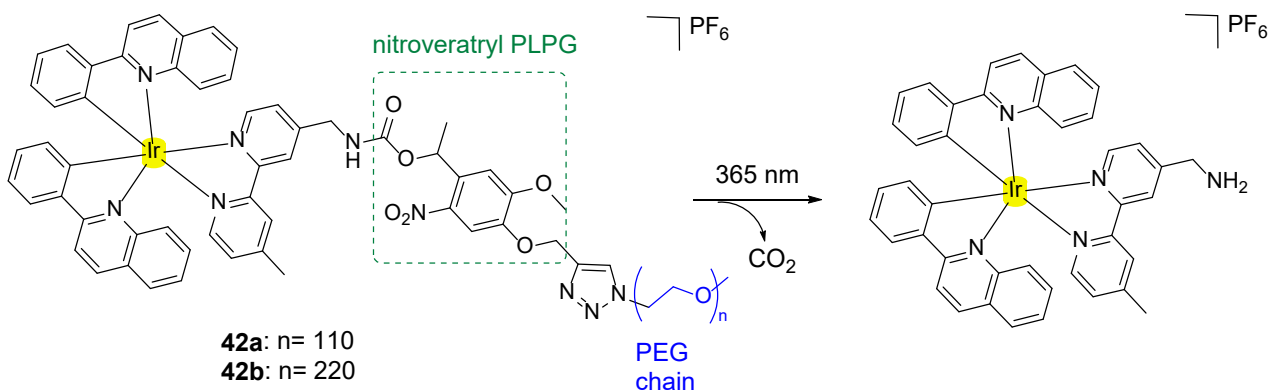
Scheme 29. Structure of **39** and its photodeprotection to form **40**.

Recently, Zhu and their co-workers developed a photoactivable carboplatin prodrug **41** linked to a BODIPY as a photoabsorber (Scheme 30).<sup>[102,103]</sup> Upon light activation, a transfer of energy occurs allowing the Pt(IV) center to be reduced.<sup>[104]</sup> The cytotoxicity of the prodrug **41** was higher on human breast carcinoma (MCF-7) cells and showed better activity under green light irradiation than carboplatin ( $IC_{50}(\mathbf{41}) = 15.7 \pm 1 \mu\text{M}$  versus  $IC_{50}(\text{carboplatin}) = 642.6 \pm 51.4 \mu\text{M}$ ). The cytotoxicity of **41** under light irradiation was 39 times higher than carboplatin alone under irradiation. The phototoxicity index (PI) of 11 expresses the better efficiency of the prodrug upon light irradiation than in the dark ( $IC_{50}(\mathbf{41}) = 173.4 \pm 8.8 \mu\text{M}$  in the dark).



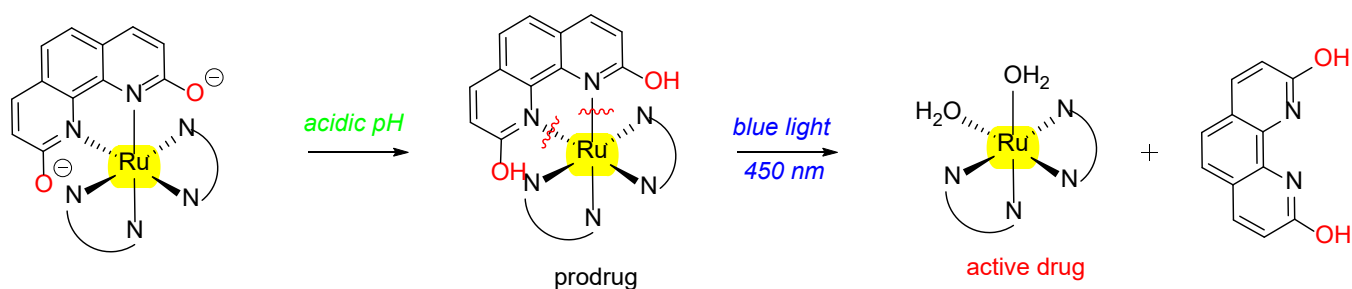
Scheme 30. Photoactivatable BODIPY-Platinum prodrug **41**.

To minimize the cytotoxicity of metal complexes in the dark, Lo and their co-workers designed photoactivatable Iridium(III) complexes **42a-b** connected to a poly(ethyleneglycol) (PEG) chain (Scheme 31).<sup>[105]</sup> The authors used a nitroveratryl group as a photolabile protecting group between the complex and the PEG chain. PEGylation was shown to significantly decrease the cytotoxicity activity of luminescent transition metal complexes.<sup>[106,107]</sup> In this study, the cytotoxicity was evaluated on HeLa cells with the irradiation wavelength at 365 nm. In the dark, compounds **42a** and **42b** were found to be less toxic than the complex alone [ $IC_{50}(\mathbf{42a}) = 36.2 \pm 3.2 \mu\text{M}$ ,  $IC_{50}(\mathbf{42b}) = 65.9 \pm 5.7 \mu\text{M}$  versus  $IC_{50}(\mathbf{Ir\ complex}) = 0.4 \pm 0.1$ ]. After 20 minutes of light irradiation, the two complexes **42a** and **42b** showed a high toxicity [ $IC_{50}(\mathbf{42a}) = 1.4 \pm 0.2 \mu\text{M}$ ,  $IC_{50}(\mathbf{42b}) = 4.9 \pm 0.1 \mu\text{M}$ ]. Interesting phototoxicity indexes of 25.9 for **42a** and 13.5 for **42b**, respectively, were obtained.



Scheme 31: Photo-release of the prodrugs **42a-b**

We note that a system combining both pH- and light-activation using a ruthenium complex was published (Scheme 32).<sup>[106]</sup> The acidic pH surrounding cancer cells activates the prodrug by weakening the bond between the phenanthroline spectator ligand and the metal center. Photodissociation then occurs under irradiation at 450 nm (blue light) releasing the active complex. This system shows promising results to minimize off targets effects (IC<sub>50</sub>: 4 μM with 450 nm light compared to cisplatin IC<sub>50</sub>: 2 μM on MCF-7 breast cancer).



Scheme 32: Ruthenium complex combining both pH- and light-activation.

#### 4. Summary and Outlook

In summary, stimuli-responsive metal-based prodrugs are promising tools to overcome the inherent drawbacks of metal-based drugs such as poor aqueous solubility, toxicity, and unfavorable biodistribution. The use of tumor-associated stimuli to selectively deliver metal complexes within malignant tissues showed promising results for both therapeutic and diagnostic applications. In this review, we reported different activation modes (endogenous or exogenous), allowing for site-specific delivery of the complexes. To date, to the best of our knowledge, none of the prodrugs discussed in this review has entered clinical trial, possibly due to a lack of activity *in vivo* or some biodistributions issues. The future directions of these prodrugs system will be to overcome these challenges by improving their accumulation in targeted tissues and controlling the release more precisely. Moreover, the exact mechanism of action or the behavior in biological environment are still not fully understood. Their understanding would certainly help to develop more efficient prodrugs. However, we are

confident that in the near future, stimuli-responsive metal-based prodrugs could become an efficient complementary method for the diagnosis and treatment of cancer.

### **Acknowledgments**

This work was financially supported by an ERC Consolidator Grant PhotoMedMet to G.G. (GA 681679), has received support under the program “Investissements d’Avenir” launched by the French Government, and was implemented by the ANR with the reference ANR-10-IDEX-0001-02 PSL (G.G.). S.P. thanks La Ligue contre le Cancer (Ligue nationale, comités Vienne and Deux-Sèvres) and La Région Nouvelle Aquitaine for their financial support.

## References

- [1] P. L. Carver, Ed., *Essential Metals in Medicine: Therapeutic Use and Toxicity of Metal Ions in the Clinic, Met. Ions Life Sci.* **2019**, *19*, 1–16.
- [2] E. J. Anthony, E. M. Bolitho, H. E. Bridgewater, O. W. L. Carter, J. M. Donnelly, C. Imberti, E. C. Lant, F. Lermyte, R. J. Needham, M. Palau, P. J. Sadler, H. Shi, F.-X. Wang, W.-Y. Zhang, Z. Zhang, *Chem. Sci.* **2020**, *11*, 12888–12917.
- [3] B. Englinger, C. Pirker, P. Heffeter, A. Terenzi, C. R. Kowol, B. K. Keppler, W. Berger, *Chem. Rev.* **2019**, *119*, 1519–1624.
- [4] K. D. Mjos, C. Orvig, *Chem. Rev.* **2014**, *114*, 4540–4563.
- [5] Chris J. Jones, John R. Thornback, *Medicinal Applications of Coordination Chemistry*, Royal Society Of Chemistry, **2007**, 201–323.
- [6] R. A. Alderden, M. D. Hall, T. W. Hambley, *J. Chem. Educ.* **2006**, *83*, 728.
- [7] P. J. Dyson, G. Sava, *Dalton Trans.* **2006**, 1929.
- [8] Chris J. Jones, John R. Thornback, *Medicinal Applications of Coordination Chemistry*, Royal Society Of Chemistry, **2007**, 324–339.
- [9] C. Orvig, M. J. Abrams, *Chem. Rev.* **1999**, *99*, 2201–2204.
- [10] M. C. Heffern, L. M. Matosziuk, T. J. Meade, *Chem. Rev.* **2014**, *114*, 4496–4539.
- [11] A. Li, C. S. Wong, M. K. Wong, C. M. Lee, M. C. Au Yeung, *BJR.* **2006**, *79*, 368–371.
- [12] V. M. Runge, *J. Magn. Reson. Imaging* **2000**, *12*, 205–213.
- [13] E. Meggers, *Chem. Commun.* **2009**, 1001.
- [14] G. Gasser, N. Metzler-Nolte, *Curr. Opin. Chem. Biol.* **2012**, *16*, 84–91.
- [15] T. Storr, K. H. Thompson, C. Orvig, *Chem. Soc. Rev.* **2006**, *35*, 534.
- [16] N. P. E. Barry, P. J. Sadler, *Chem. Commun.* **2013**, *49*, 5106.
- [17] J. Spencer, B. Walden, *Future Med. Chem.* **2018**, *10*, 607–609.
- [18] T. Fuereder, W. Berger, *ESMO Open* **2017**, *2*, e000239.
- [19] Y. Xue, H. Bai, B. Peng, B. Fang, J. Baell, L. Li, W. Huang, N. H. Voelcker, *Chem. Soc. Rev.* **2021**, *50*, 4872–4931.
- [20] C. Sanchez-Cano, M. J. Hannon, *Dalton Trans.* **2009**, 10702.
- [21] A. Albert, *Nature* **1958**, *182*, 421–423.
- [22] R. Walther, J. Rautio, A. N. Zelikin, *Adv. Drug Deliv. Rev.* **2017**, *118*, 65–77.
- [23] X. Wang, X. Wang, S. Jin, N. Muhammad, Z. Guo, *Chem. Rev.* **2019**, *119*, 1138–1192.
- [24] J. Z. Drago, S. Modi, S. Chandarlapaty, *Nat Rev Clin Oncol* **2021**, *18*, 327–344.
- [25] S. Baah, M. Laws, K. M. Rahman, *Molecules* **2021**, *26*, 2943.
- [26] B. G. de la Torre, F. Albericio, *Molecules* **2021**, *26*, 627.
- [27] N. Graf, S. J. Lippard, *Adv. Drug Deliv. Rev.* **2012**, *64*, 993–1004.
- [28] S. H. van Rijt, P. J. Sadler, *Drug Discov. Today* **2009**, *14*, 1089–1097.
- [29] S. M. Meier-Menches, C. Gerner, W. Berger, C. G. Hartinger, B. K. Keppler, *Chem. Soc. Rev.* **2018**, *47*, 909–928.
- [30] E. Alessio, L. Messori, *Molecules* **2019**, *24*, 1995.
- [31] G. P. Stathopoulos, T. Boulikas, *J. Drug Deliver.* **2012**, *2012*, 1–10.
- [32] J. Karges, *Angew. Chem. Intl. Edit.* **2022**, *61*, e202112236.
- [33] S. A. McFarland, A. Mandel, R. Dumoulin-White, G. Gasser, *Curr. Opin. Chem. Biol.* **2020**, *56*, 23–27.
- [34] M. Graaf, E. Boven, H. Scheeren, H. Haisma, H. Pinedo, *CPD.* **2002**, *8*, 1391–1403.
- [35] D. Niculescu-Duvaz, G. Negoita-Giras, I. Niculescu-Duvaz, D. Hedley, C. J. Springer, *Methods and Principles in Medicinal Chemistry.* **2011**, 271–344. [36] R. A. Moats, S. E. Fraser, T. J. Meade, *Angew. Chem. Intl. Ed. Engl.* **1997**, *36*, 726–728.
- [37] A. Y. Louie, M. M. Hüber, E. T. Ahrens, U. Rothbacher, R. Moats, R. E. Jacobs, S. E. Fraser, T. J. Meade, *Nat. Biotechnol.* **2000**, *18*, 321–325.

- [38] M. M. Alauddin, A. Y. Louie, A. Shahinian, T. J. Meade, P. S. Conti, *Nucl. Med. Biol.* **2003**, *5*.
- [39] L. M. Lilley, S. Kamper, M. Caldwell, Z. K. Chia, D. Ballweg, L. Vistain, J. Krimmel, T. A. Mills, K. MacRenaris, P. Lee, E. A. Waters, T. J. Meade, *Angew. Chem.* **2020**, *132*, 396–402.
- [40] Y.-T. Chang, C.-M. Cheng, Y.-Z. Su, W.-T. Lee, J.-S. Hsu, G.-C. Liu, T.-L. Cheng, Y.-M. Wang, *Bioconjugate Chem.* **2007**, *18*, 1716–1727.
- [41] T. Chauvin, P. Durand, M. Bernier, H. Meudal, B.-T. Doan, F. Noury, B. Badet, J.-C. Beloeil, É. Tóth, *Angew. Chem. Int. Ed.* **2008**, *47*, 4370–4372.
- [42] T. Chauvin, S. Torres, R. Rosseto, J. Kotek, B. Badet, P. Durand, É. Tóth, *Chem. Eur. J.* **2012**, *18*, 1408–1418.
- [43] A. Keliris, I. Mamedov, G. E. Hagberg, N. K. Logothetis, K. Scheffler, J. Engelmann, *Contrast Media Mol. Imaging* **2012**, *7*, 478–483.
- [44] S. Mizukami, H. Matsushita, R. Takikawa, F. Sugihara, M. Shirakawa, K. Kikuchi, *Chem. Sci.* **2011**, *2*, 1151.
- [45] Z. Zeng, S. Mizukami, K. Kikuchi, *Anal. Chem.* **2012**, *84*, 9089–9095.
- [46] Z. Zeng, S. Mizukami, K. Fujita, K. Kikuchi, *Chem. Sci.* **2015**, *6*, 4934–4939.
- [47] J. A. Duimstra, F. J. Femia, T. J. Meade, *J. Am. Chem. Soc.* **2005**, *127*, 12847–12855.
- [48] R. A. Tromp, S. S. G. E. van Boom, C. Marco Timmers, S. van Zutphen, G. A. van der Marel, H. S. Overkleeft, J. H. van Boom, J. Reedijk, *Bioorg. Med. Chem. Lett.* **2004**, *14*, 4273–4276.
- [49] I. Tranoy-Opalinski, T. Legigan, R. Barat, J. Clarhaut, M. Thomas, B. Renoux, S. Papot, *Eur. J. Med. Chem.* **2014**, *74*, 302–313.
- [50] H. Matsushita, S. Mizukami, Y. Mori, F. Sugihara, M. Shirakawa, Y. Yoshioka, K. Kikuchi, *ChemBioChem.* **2012**, *13*, 1579–1583.
- [51] S. Hanessian, J. Wang, *Can. J. Chem.* **1993**, *71*, 896–906.
- [52] S. Bauhuber, C. Hozsa, M. Breunig, A. Göpferich, *Advanced Materials* **2009**, *21*, 3286–3306.
- [53] P. Ruzza, A. Calderan, *Pharmaceutics* **2013**, *5*, 220–231.
- [54] J. Zhang, X. Bao, J. Zhou, F. Peng, H. Ren, X. Dong, W. Zhao, *Biosensors and Bioelectronics* **2016**, *85*, 164–170.
- [55] M. Porubský, S. Gurská, J. Stanková, M. Hajdúch, P. Džubák, J. Hlaváč, *RSC Adv.* **2019**, *9*, 25075–25083.
- [56] R. G. Kenny, S. W. Chuah, A. Crawford, C. J. Marmion, *Eur. J. Inorg. Chem.* **2017**, *2017*, 1596–1612.
- [57] Z. Wang, Z. Deng, G. Zhu, *Dalton Trans.* **2019**, *48*, 2536–2544.
- [58] T. W. Hambley, *J. Biol. Inorg. Chem.* **2019**, *24*, 457–466.
- [59] X. Wang, Z. Guo, *Chem. Soc. Rev.* **2013**, *42*, 202–224.
- [60] H. Yao, G. Zhu, *Dalton Trans.* **2022**, *51*, 5394–5398.
- [61] Z. Yang, H. Lin, J. Huang, A. Li, C. Sun, J. Richmond, J. Gao, *Chem. Commun.* **2019**, *55*, 4546–4549.
- [62] S. Chen, X. Zhao, J. Chen, J. Chen, L. Kuznetsova, S. S. Wong, I. Ojima, *Bioconjugate Chem.* **2010**, *21*, 979–987.
- [63] E. Kinski, P. Marzenell, W. Hofer, H. Hagen, J. A. Raskatov, K. X. Knaup, E. M. Zolnhofer, K. Meyer, A. Mokhir, *J. Inorg. Biochem.* **2016**, *160*, 218–224.
- [64] P. Marzenell, H. Hagen, L. Sellner, T. Zenz, R. Grinyte, V. Pavlov, S. Daum, A. Mokhir, *J. Med. Chem.* **2013**, *56*, 6935–6944.
- [65] T. Sun, T. Lv, J. Wu, M. Zhu, Y. Fei, J. Zhu, Y. Zhang, Z. Huang, *J. Med. Chem.* **2020**, *acs.jmedchem.0c01435*.
- [66] V. E. Y. Lee, Z. C. Lim, S. L. Chew, W. H. Ang, *Inorg. Chem.* **2021**, *60*, 1823–1831.

- [67] A. K. Renfrew, N. S. Bryce, T. W. Hambley, *Chem. Sci.* **2013**, *4*, 3731.
- [68] N. Yamamoto, A. K. Renfrew, B. J. Kim, N. S. Bryce, T. W. Hambley, *J. Med. Chem.* **2012**, *55*, 11013–11021.
- [69] M. D. Hall, T. W. Failes, N. Yamamoto, T. W. Hambley, *Dalton Trans.* **2007**, 3983.
- [70] Swietach P, Vaughan-Jones RD, Harris AL, Hulikova A. **2014** The chemistry, physiology and pathology of pH in cancer. *Phil. Trans. R. Soc. B* 369: 20130099.
- [71] L. Frullano, B. Tejerina, T. J. Meade, *Inorg. Chem.* **2006**, *45*, 8489–8491.
- [72] G.L. Beretta · F. Zunino, K, Anthracycline Chemistry and Biology II, *Top Curr Chem.* **2008**, *283*, 1-206.
- [73] L. Frullano, B. Tejerina, T. J. Meade, *Inorg. Chem.* **2006**, *45*, 8489–8491.
- [74] K. Na, S. A. Lee, S. H. Jung, B. C. Shin, *Colloids and Surfaces B: Biointerfaces* **2011**, *84*, 82–87.
- [75] M. I. Webb, B. Wu, T. Jang, R. A. Chard, E. W. Y. Wong, M. Q. Wong, D. T. T. Yapp, C. J. Walsby, *Chem. Eur. J.* **2013**, *19*, 17031–17042.
- [76] Y. Zhang, A. Ho, J. Yue, L. Kong, Z. Zhou, X. Wu, F. Yang, H. Liang, *Eur. J. Med. Chem.* **2014**, *86*, 449–455.
- [77] I. N. Stepanenko, A. Casini, F. Edefe, M. S. Novak, V. B. Arion, P. J. Dyson, M. A. Jakupec, B. K. Keppler, *Inorg. Chem.* **2011**, *50*, 12669–12679.
- [78] J. Qi, Y. Gou, Y. Zhang, K. Yang, S. Chen, L. Liu, X. Wu, T. Wang, W. Zhang, F. Yang, *J. Med. Chem.* **2016**, *59*, 7497–7511.
- [79] Y. Zhang, Z. Zhang, Y. Gou, M. Jiang, H. Khan, Z. Zhou, H. Liang, F. Yang, *J. Inorg. Biochem.* **2017**, *172*, 1–8.
- [80] Y. Gou, J. Qi, J.-P. Ajayi, Y. Zhang, Z. Zhou, X. Wu, F. Yang, H. Liang, *Mol. Pharmaceutics* **2015**, *12*, 3597–3609.
- [81] J. Qi, Y. Zhang, Y. Gou, Z. Zhang, Z. Zhou, X. Wu, F. Yang, H. Liang, *Mol. Pharmaceutics* **2016**, *13*, 1501–1507.
- [82] F. Yang, H. Liang, *Future Med. Chem.* **2016**, *8*, 89–91.
- [83] Y. Gou, Y. Zhang, J. Qi, Z. Zhou, F. Yang, H. Liang, *J. Inorg. Biochem.* **2015**, *144*, 47–55.
- [84] Y. Gou, Z. Zhang, J. Qi, S. Liang, Z. Zhou, F. Yang, H. Liang, *J. Inorg. Biochem.* **2015**, *153*, 13–22.
- [85] Y. Gou, Y. Zhang, Z. Zhang, J. Wang, Z. Zhou, H. Liang, F. Yang, *Mol. Pharmaceutics* **2017**, *14*, 1861–1873.
- [86] J. Delahousse, C. Skarbek, A. Paci, *Cancer Chemother. Pharmacol.* **2019**, *84*, 937–958.
- [87] H. Hagen, P. Marzenell, E. Jentzsch, F. Wenz, M. R. Veldwijk, A. Mokhir, *J. Med. Chem.* **2012**, *55*, 924–934.
- [88] M. Schikora, A. Reznikov, L. Chaykovskaya, O. Sachinska, L. Polyakova, A. Mokhir, *Bioorg. Med. Chem. Lett.* **2015**, *25*, 3447–3450.
- [89] S. Daum, M. S. V. Reshetnikov, M. Sisa, T. Dumych, M. D. Lootsik, R. Bilyy, E. Bila, C. Janko, C. Alexiou, M. Herrmann, L. Sellner, A. Mokhir, *Angew. Chem. Int. Ed.* **2017**, *56*, 15545–15549.
- [90] V. Reshetnikov, S. Daum, C. Janko, W. Karawacka, R. Tietze, C. Alexiou, S. Paryzhak, T. Dumych, R. Bilyy, P. Tripal, B. Schmid, R. Palmisano, A. Mokhir, *Angew. Chem. Int. Ed.* **2018**, *57*, 11943–11946.
- [91] V. Reshetnikov, H. G. Özkan, C. Alexiou, C. Sauer, M. R. Heinrich, A. Mokhir, **2020**, *25*, 2545.
- [92] V. Reshetnikov, S. Daum, A. Mokhir, *Chem. Eur. J.* **2017**, *23*, 5678–5681.
- [93] V. Reshetnikov, A. Arkhypov, P. R. Julakanti, A. Mokhir, *Dalton Trans.* **2018**, *47*, 6679–6682.
- [94] J.-A. Cuello-Garibo, M. S. Meijer, S. Bonnet, *Chem. Commun.* **2017**, *53*, 6768–6771.



- [95] S. Bonnet, *Dalton Trans.* **2018**, 47, 10330–10343.
- [96] T. Joshi, V. Pierroz, C. Mari, L. Gemperle, S. Ferrari, G. Gasser, *Angew. Chem. Int. Ed.* **2014**, 53, 2960–2963.
- [97] V. Pierroz, T. Joshi, A. Leonidova, C. Mari, J. Schur, I. Ott, L. Spiccia, S. Ferrari, G. Gasser, *J. Am. Chem. Soc.* **2012**, 134, 20376–20387.
- [98] A. Leonidova, V. Pierroz, R. Rubbiani, Y. Lan, A. G. Schmitz, A. Kaech, R. K. O. Sigel, S. Ferrari, G. Gasser, *Chem. Sci.* **2014**, 5, 4044.
- [99] C. Mari, V. Pierroz, A. Leonidova, S. Ferrari, G. Gasser, *Eur. J. Inorg. Chem.* **2015**, 2015, 3879–3891.
- [100] A. Leonidova, C. Mari, C. Aebersold, G. Gasser, *Organometallics* **2016**, 35, 851–854.
- [101] J. Kasparkova, H. Kostrhunova, O. Novakova, R. Křikavová, J. Vančo, Z. Trávníček, V. Brabec, *Angew. Chem. Int. Ed.* **2015**, 54, 14478–14482.
- [102] H. Yao, S. Chen, Z. Deng, M.-K. Tse, Y. Matsuda, G. Zhu, *Inorg. Chem.* **2020**, 59, 11823–11833.
- [103] H. Yao, Y. F. Gunawan, G. Liu, M.-K. Tse, G. Zhu, *Dalton Trans.* **2021**, 50, 13737–13747.
- [104] Z. Dai, Z. Wang, *Molecules* **2020**, 25, 5167.
- [105] K. K.-S. Tso, K.-K. Leung, H.-W. Liu, K. K.-W. Lo, *Chem. Commun.* **2016**, 52, 4557–4560.
- [106] S. P.-Y. Li, C. T.-S. Lau, M.-W. Louie, Y.-W. Lam, S. H. Cheng, K. K.-W. Lo, *Biomaterials* **2013**, 34, 7519–7532.
- [107] A. W.-T. Choi, M.-W. Louie, S. P.-Y. Li, H.-W. Liu, B. T.-N. Chan, T. C.-Y. Lam, A. C.-C. Lin, S.-H. Cheng, K. K.-W. Lo, *Inorg. Chem.* **2012**, 51, 13289–13302.

## Table of Contents

1. Introduction.....	6
2. Enzyme-responsive metal complexes .....	10
2.1. $\beta$ -Galactosidase.....	10
a. Imaging.....	10
2.2. $\beta$ -Glucuronidase .....	18
a. Imaging.....	18
b. Therapy.....	19
2.3. $\beta$ -Lactamase.....	20
a. Imaging .....	20
b. Therapy.....	20
3. Others triggers.....	22
3.1. Chemical reduction /redox activation.....	22
a. Imaging.....	22
b. Therapy.....	25
3.2. Acidic pH activation.....	31
3.3. Activation by the high production of ROS .....	34
3.4. Photo-deprotection.....	38
4. Summary and Outlook .....	43

## Graphical Abstract

**Let's make metal-based drugs more selective!** The main advances in the use of metal-based prodrugs are discussed in this review.

